
Quorum Sensing in Bacterial Biofilms

Regulating Matrix Production through Communication

Author: Avaneesh Venkata Narla

Adviser: Professor Ned Wingreen

Second Reader: Professor Bonnie Bassler



A SENIOR THESIS SUBMITTED IN PARTIAL FULFILLMENT
OF THE REQUIREMENTS FOR THE DEGREE OF BACHELOR OF ARTS IN PHYSICS
AT PRINCETON UNIVERSITY

2017

© Copyright 2017 by Avaneesh Venkata Narla.

All rights reserved.

I pledge my honor that this represents my own original work in accordance with
Princeton University regulations.

A handwritten signature in black ink, appearing to read "Avaneesh Venkata Narla". The signature is fluid and cursive, with a long horizontal line underneath it.

Avaneesh Venkata Narla

మమైలు, నీ కోసం

Abstract

Bacteria grow on surfaces in complex communities known as biofilms. Biofilms are composed of cells embedded in extracellular matrix. Within biofilms, bacteria often communicate, cooperate, and compete within their own species and with other species using Quorum Sensing (QS). QS refers to the process by which bacteria produce, secrete, and subsequently detect small molecules called autoinducers (AIs) to assess the local population density of their species, or of other species. QS is known to regulate the production of extracellular matrix. We investigated the benefit of QS in regulating matrix production to gain access to a nutrient that diffuses from a source far from the biofilm. We employed Agent-Based Modeling (ABM), a simulation framework that allows cells to modify their behavior based on local inputs, e.g. nutrient and AI concentrations. We first determined the optimal fixed strategies (that do not use QS) for simulated pairwise competitions between strains, and identified the conditions that favor matrix production. To understand if QS can provide a competitive advantage, we modified our model to include QS with constitutive AI production. We demonstrated that simple QS-based strategies can be superior to any fixed strategy. However, we found that if AI production is not constitutive but rather depends on nutrient intake, then QS-based strategies fail to provide an advantage. We explain this failure of QS using analytic methods. We derive an expression for the biophysically limited dynamic range of AI concentration detection in nutrient limited environments. This expression implies that for QS to provide an advantage in biofilms, production of AI should be privileged and not limited by overall metabolic rates.

Acknowledgements

This thesis is a culmination of one and half years of research, and the number of people who have contributed to it in one way or the other is immense. It truly takes a village to write a thesis. Though their names may be absent here, I am grateful to them for giving me their time and changing me in the process.

I started this section by thanking Ned. But before I had finished, I was already running into my fourth page. While it would take much more than four pages to even begin thanking Ned, the first sentence of what I wrote succinctly expresses the sentiment spanning my appreciation for and gratitude toward Ned: When people ask me how I like working with my adviser, I invariably reply, “Asking Ned if I could work with him has been the best decision that I have made at Princeton”. And my conviction in that response has only grown over time. Perhaps the only reason that I decided to pursue a PhD after graduation (and I came close to not doing so) is because of the influence that Ned has had on me. Ned has been more of an adviser, mentor, guide, teacher, friend and inspiration to me than I could have ever imagined in my most fantastical of dreams. I am forever indebted to him for his selflessness.

This scientific project is the fruit of an extensive series of conversations that emphasizes the multidisciplinary nature of the endeavor. It is an understatement to say that this project was only possible because of incredible work done by David Borenstein, Jing Yan, and Matt Jemielita; and their willingness to train the novice who knocked on their doors incessantly. It is as much the fruit of their expertise and patience as my labor and I would have been helpless without their guidance. I would also like to thank Prof. Bonnie Bassler for valuable conversations, and for agreeing to be a second reader for this thesis; and Farzan Beroz for guiding me in tackling mathematical hurdles. I also thank the CSES team at PICSciE who took the time to

teach me the tricks and tools behind using the Della cluster, and went out of their way to teach me C and other programming tools. This project was heavily reliant on the computing infrastructure and the support that PICSciE provided.

But none of the science would have been possible if I did not have the constant support from all my friends. My closest friends, Jen, Char and Aaron, have been there every step of the way, going back to 2012 when we spent a year in Peru together. I would also like to thank all other members of the Bridge Year family. For an international student who struggled to assimilate, this community has been incredibly supportive and a defining feature of my Princeton experience. I can only hope that distance will be no barrier in the future and that our friendships continue to grow.

Some of my fondest memories at Princeton have been times spent with my roommates: James, Josh, Justin, and Robby in my freshman year; And Claire, Doug, Kenny, and Neeta in my junior year. I will always fondly remember the crosswords, home-cooked dinners, runs and late-night conversations. And finally, being a physics major might not have been possible without Jason Manley, and it definitely would not have been even marginally as fun.

I would also like to thank three spaces. Firstly, long hours of work would not have been possible without beautiful runs on the tow path. Secondly, 2D has been the most special place on campus for me, and if I could stay in 2D for the rest of my life, I would do so in a heartbeat. The people, the food, the party with PSafe, everything; it has been a home away from home. And finally, Princeton. I am not ready to leave this June, and the stars will receive endless gratitude for dropping me here (in lieu of the alumni donations that I cannot afford as a graduate student).

And most of all, I would like to thank my family. 8,000 miles cannot stop the love of my parents, my brother and my grandmother from reaching me and keeping me going every day. I am blessed and can only hope to repay the endless love that I have received from my family while I pursuing my ambitions. Words fail miserably in any effort to thank them.

Contents

Abstract	v
Acknowledgements	vi
Contents	viii
List of Figures	xi
List of Tables	xiv
1 Introduction	1
1.1 Bacterial Biofilms	1
1.2 Quorum Sensing	4
1.3 Applications	6
1.4 Previous Work	7
1.5 Simulation Framework	9
1.5.1 Agent-Based Modeling	9
1.5.2 ABM for Biofilm Modeling	10
1.5.3 Nanoverse	11
2 Methodology	13
2.1 Pairwise Competitions	13
2.2 Geometry of Simulations	14
2.3 Initial Placement of Bacteria	14
2.4 Influx of Nutrient	15
2.5 Boundary Conditions	16

2.6	Reaction Diffusion Equation	17
2.7	Reproduction and Production of Matrix	18
2.8	Shoving Algorithm	18
2.9	Discussion of Parameters	20
3	Optimizing Matrix Production without QS	23
3.1	Reproduction and Matrix Production	23
3.2	Results and Discussion	24
3.2.1	Pair-wise Competitions	24
3.2.2	Time Dependence	27
3.2.3	Margins of Advantage	29
4	The Role of Quorum Sensing	32
4.1	Constitutive Autoinducer Production	32
4.2	Autoinducer Detection	33
4.3	Discussion of Parameters	34
4.4	Results and Discussion	35
5	Oxygen-dependent AI Production	38
5.1	Biological Motivation	38
5.2	Methodology	39
5.3	Discussion of Parameters	40
5.4	Results and Discussion	41
5.5	Analytic Derivation of the Biophysical Limit for the Dynamic Range of Quorum Sensing in Three Dimensions	45
6	Conclusion	50
6.1	Summary of Results	50
6.2	Reconciling QS and the Biophysics Limit	50
6.3	Assumptions behind the Agent-Based Model	52

6.4	Limitations and Future Steps	53
6.5	Experimental Verification	54
7	References	55
	Appendices	61
	A Supplementary Information	62
A.1	The Algorithm behind Nanoverse	62
A.2	Solving the Reaction-Diffusion Equation	62
A.2.1	Superposition Method	63
A.2.2	Linear Solvers	64
B	Supplementary Figures	65
B.1	Parameter Dependence for Fixed Strategies	69
C	Afterword on Relating Computer Models to Real Biological Systems	73

List of Figures

1.1	5 stages of Biofilm Maturation	2
1.2	A contour map of O ₂ concentrations around a biofilm cell cluster	3
1.3	The mechanism of quorum sensing activation	6
1.4	Fire escape agent-based simulation	10
1.5	Presence of cheaters growing among producer cells in a static culture of <i>Vibrio cholerae</i>	11
2.1	A zoomed-in snippet of a snapshot of the simulation	14
2.2	A zoomed-in snippet of the bottom of the simulation domain at ini- tialization	15
2.3	A snapshot of a simulation indicating the influx of oxygen	16
2.4	Demonstration of the shoving algorithm used for matrix production and reproduction	20
3.1	Snapshots of a pairwise competition between fixed-strategies	24
3.2	Mean of the logarithm of the ratio of number of cells for fixed strategies at the end of the simulation	25
3.3	Number of simulations completed for each pair of fixed strategies . .	26
3.4	Standard Deviation of logarithm of ratio for each pair of fixed strategies	26
3.5	The progression of the mean of the log of the ratio of numbers of fixed strategies over time	28
3.6	Fixed strategies of matrix bias 0.2 and 0.7 against other fixed strategies	30

3.7	Snapshots from simulations showing large margin of victory by low but successful matrix bias as opposed to smaller margin of victory by high matrix bias for fixed strategies	31
4.1	Model of constitutive autoinducer production	33
4.2	The forms of r_r and r_m for different values of local autoinducer concentration	34
4.3	Snapshots of a pairwise competition between constitutive AI producing QS strategy and a fixed strategy	36
4.4	Mean of the logarithm of the ratio of number of cells for QS strategies in competition with fixed strategies	37
5.1	Model of oxygen-dependent autoinducer production	40
5.2	Snapshots of a pairwise competition between nutrient-dependent AI producing QS strategy and fixed-strategies	41
5.3	Mean of the logarithm of the ratio of number of cells for a QS strategy with nutrient-dependent AI-production in competition with fixed strategies	43
5.4	Maximum AI concentration over time for constitutive AI production and nutrient-dependent AI production	44
B.1	Mean of log of ratio of matrix produced by strategy A to the matrix produced by strategy A	65
B.2	Standard Deviation of log of ratio of matrix produced by strategy A to the matrix produced by strategy A	66
B.3	Mean of log of ratio of biomass of strategy A to the biomass of strategy A	67
B.4	The mean number of timesteps required to reach the halt condition for pairwise competitions between fixed strategies	68
B.5	The standard deviation of the number of timesteps required to reach the halt condition for pairwise competitions between fixed strategies .	68

B.6	Results for fixed strategies with 32 cells of each strategy	69
B.7	Results for fixed strategies with a relative cost of 3 for reproduction to matrix production	70
B.8	Results for fixed strategies with a diffusion constant of 0.01	71
B.9	Results for fixed strategies with a rate of nutrient consumption of 0.005	72

List of Tables

2.1	Parameters for processes in the time scale of reproduction	21
2.2	Parameters for processes in the time scale of equilibration for the reaction-diffusion equation	22
4.1	Parameters used to incorporate QS into the simulation	35

Chapter 1

Introduction

Note: Parts of this chapter have been adapted (in accordance with University regulations) from the Junior Paper written for the Physics Department by the author in the Spring semester of the academic year 2015-2016.

1.1 Bacterial Biofilms

Bacteria do not generally exist in nature as homogenously dispersed single cells, but instead accumulate at interfaces to form polymicrobial aggregates [1]. Many species of bacteria form immobile communities with large numbers of densely packed cells [2]. These communities are called biofilms and usually form on surfaces or at air-liquid interfaces. Bacterial biofilms may adhere to biological or non-biological surfaces, and are ubiquitous in nature; they are found environments as diverse as hot springs and deep-sea vents [3].

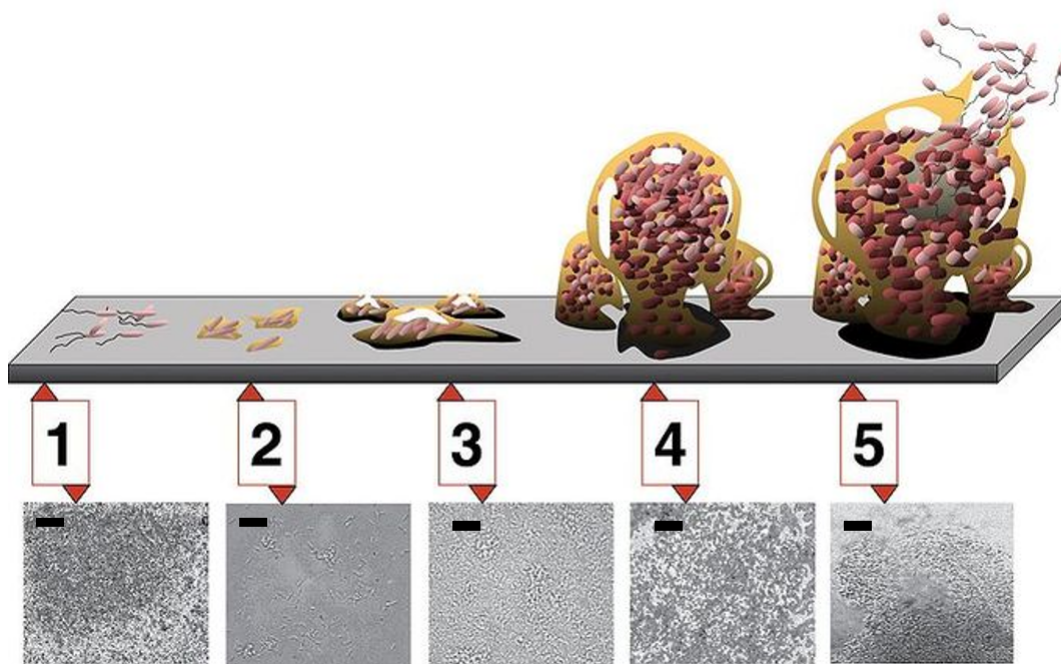


Figure 1.1: Biofilm maturation typically occurs in 5 stages. Stage 1: Attachment of planktonic bacteria to surface. Stage 2: Aggregation and irreversible attachment through matrix production. Stage 3: Growth, division, and continued matrix production. Stage 4: Mature biofilm. Stage 5: Dispersal of a part of the biofilm into planktonic bacteria. Each stage of development in the diagram is paired with a photomicrograph of a developing *Pseudomonas aeruginosa* biofilm. All photomicrographs are shown to the same scale (the bar scales to 10 μm). Figure reproduced from [4].

Cells in biofilms are held together by an extra-cellular matrix, which is usually composed of polysaccharides, protein, and DNA [5]. The extra-cellular matrix provides protection from external threats such as antimicrobial compounds and predatory organisms, facilitates horizontal gene transfer, and affords many other advantages [6]. Matrix production can also help the bacteria collectively grow toward nutrient sources. Nutrients, such as oxygen, diffuse in from a source far away from the bacteria. The cells closer to the nutrient source, at the edge of the biofilm, have greater access to nutrients and consume a large proportion of the nutrients (which facilitates a higher

growth rate). As a result, the concentration of nutrients is typically very low at the center of a biofilm cell cluster (Fig. 1.2). Bacteria shove other bacterial cells to the edge of the biofilm by reproducing and producing matrix. As producing matrix is significantly cheaper per unit volume than reproducing, bacteria can gain a competitive advantage in accessing nutrient by allocating a proportion of resources to matrix production [7]. We will call the fraction of resources allocated to matrix production the *matrix bias* of the bacteria. In our investigation, we explore bacteria of different matrix production strategies that differ in their matrix biases.

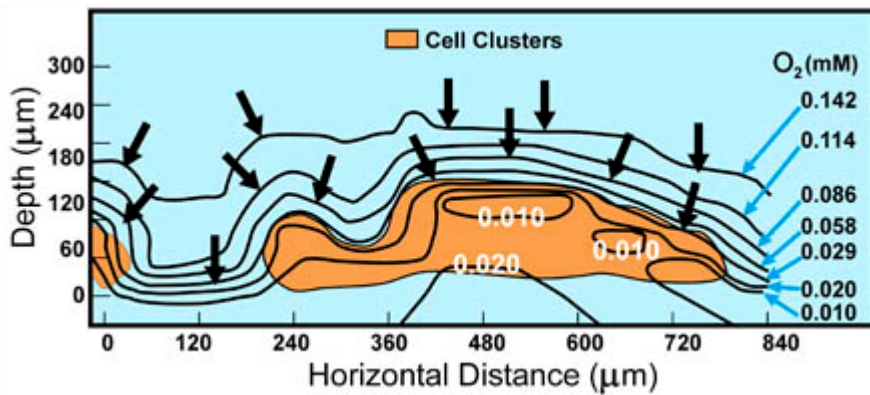


Figure 1.2: A contour map of O_2 concentrations around a biofilm cell cluster. The cross-sectional map was constructed based on several oxygen microsensor profiles of a small region of a biofilm. The substratum is at the bottom (depth = 0) and the bulk fluid containing O_2 at the top. The arrows indicate the direction of the local diffusive flux of O_2 . Figure adapted from [8].

However, allocating resources to matrix production, and away from reproduction, lowers the growth rate of the bacteria at any fixed concentration of nutrient. Further, matrix production affords no benefit in accessing the nutrient for the group of cells as a whole when there is no competition from other groups. This is because, collectively, the group benefits from maximizing its growth rate: there is no net collective benefit to the group if one member of the group is shoved to the edge of the biofilm before another member of the group. Therefore, producing matrix is not always beneficial,

and regulation of matrix production in different situations can impart significant competitive advantages.

Thus, there is a trade-off between producing matrix, which allows bacteria to gain a competitive advantage over other bacteria in accessing nutrient, and reproducing, which increases the growth rate for a given concentration of nutrient. We hypothesize that, through evolution, bacteria find the optimal matrix bias that maximizes *evolutionary fitness* in different conditions. We aim to understand the different factors that affect the value of optimal matrix bias, and consequently how the matrix bias would be affected by different conditions. To this end, we investigated whether communication between bacterial cells can help the bacteria gain a competitive advantage over bacteria with strategies that do not communicate to modify their matrix bias.

As part of our investigation, we sought the optimal matrix bias for a growing biofilm in nutrient-limited environments through simulations of biofilms. We first considered the case where the cells have a fixed matrix bias, and then we considered a case where cells could communicate by means of chemical signals in order to regulate matrix production. The form of bacterial communication considered is called quorum sensing.

1.2 Quorum Sensing

In the 1960s and 1970s, it was discovered that bacteria are capable of communicating with their neighbors through a process now known as quorum sensing (QS). QS is mediated by the production and detection of chemical signals known as autoinducers (AIs) that are secreted into the environment [5].

The mechanism of QS can be explained in a simplified manner as follows. Each individual cell produces AI, even in the absence of other cells. As the population of quorum-sensing bacteria in a given volume increases, the concentration of AI in the given volume increases. When the local AI concentration crosses a certain threshold,

the individual cells respond with an alteration in their gene expression (Fig. 1.3). As nearby cells will detect a similar local AI concentration, the alteration in gene expression is population-wide [5]. Often, AI molecules induce further production of AI by the bacteria, which is the origin of the name “autoinducer”.

This mechanism allows bacteria to control processes that are unproductive when undertaken by an individual but effective when undertaken by all members of the group. A good example of this is bioluminescence. *Aliivibrio fischeri*, a bacterium found in the sea, is known to produce an enzyme, luciferase, that causes bioluminescence by the oxidation of organic compounds. The bioluminescence generated would not be detectable if produced by a single cell but is detectable when produced by a large number of cells [9]. Thus, QS prevents the bacteria from wasting resources and energy to produce the bioluminescence enzyme when at low cell densities, but still allows them to behave as multicellular organisms and reap the benefits of cooperation and organization when at high densities. Other examples of processes controlled by QS are virulence factor secretion, biofilm formation, and sporulation [5].

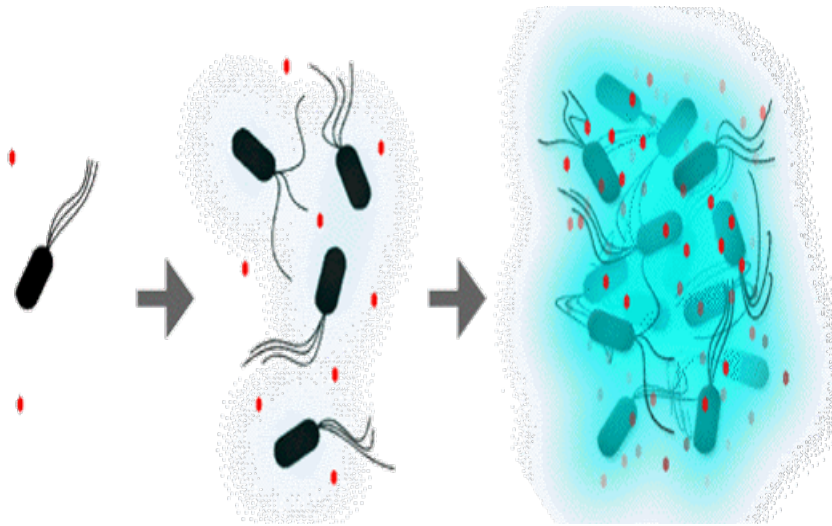


Figure 1.3: The mechanism of QS activation: At low cell densities (left-most figure), cells produce AIs, but as cells do not detect a high AI concentration, there is no change in gene expression. At high cell densities (right-most figure), there is an accumulation of AIs and the cells respond to the high AI concentration with a population-wide change in gene expression (in this case, bioluminescence). Figure adapted from [10].

1.3 Applications

The ubiquity of bacterial biofilms in nature means that a greater understanding of the spatial features and competitive advantages of bacterial biofilms can lead to many different applications. For example, to target virulent bacteria in the human body, promoting competition between species (by using probiotics) can lead to a reduction in the success of virulent bacteria and hence the severity of infections [7]. In another example, spatial segregation can be used in the biofilms of wastewater treatment reactors. In such reactors, O_2 is supplied at low levels, such that it is fully consumed by the bacteria in the outer layers [7].

Understanding the role of QS can also have many applications in antibiotic and probiotic interventions. As QS is mediated by chemical signals (AIs), understanding

QS can allow treatments in a target system through the fabrication and introduction of artificial chemicals that interfere or manipulate the target system's signaling. Furthermore, understanding the mechanisms of AI production can help target the viability of the quorum-sensing bacteria. Targeting the AI production mechanism allows for a wide range of new interventions. Such applications are particularly useful in bacterial systems where targeting other biological processes has failed. In this report, we will demonstrate a biophysical limit to QS. We hope that this biophysical limit will provide a deeper understanding of the mechanisms behind AI production. Targeting the mechanisms of AI production can be an effective means of defending a host against virulent bacteria, as AI production can be essential to virulence. The biophysical limit will also help us understand the different ecological regimes in which QS is relevant.

1.4 Previous Work

Much work has been done using simulation models to understand the role of matrix production. Xavier and Foster (2007) used simulations with O₂ gradients originating from diffusion-reaction models. In their simulations, a bulk O₂ concentration was placed away from an initial seed of cells. They found that investment in matrix production provided a relative fitness to matrix-producing bacteria over bacteria that produced no matrix [11]. They also performed an invasion analysis of matrix production as a continuous trait. That is, they compared bacteria with a matrix bias of f with bacteria with a matrix bias of $f - \Delta f$. For their set of parameters, they found that the bacteria of higher matrix bias won if $f \leq 0.7$ [11]. A few things to note of their methodology is that they used simulations with a continuous 2D geometry and did not compare strategies of vastly different matrix biases.

Nadell et al. (2008) incorporated QS using a constant AI production model. In their simulations, all cells produced AI constantly, and when the cells detected an

AI concentration over a certain threshold, the cells stopped producing matrix. In simulations of pairwise competitions, they found that QS provides an advantage for matrix-producing cells. This advantage was visible once the QS cells gained enough of a competitive advantage such that they were the only cells with access to the nutrient. The QS cells thus did not have to compete for nutrients and deactivation of polymer production yielded an advantage by redirecting resources into growth. They found that, at short times, cells using QS performed better than matrix-producing cells not using QS [12]. However, at long times, constitutive matrix production performed better. Once the QS cells stopped producing matrix, they could grow very quickly, but at long times lost their privileged access to the nutrient. Despite having less access to nutrients, the non-QS cells (that constitutively produced matrix) generated more volume of biomass than the QS cells due to the low cost of producing matrix. Biomass production shoved the non-QS cells toward the nutrient source, and they slowly regained access to nutrients. Thus, at long times, the non-QS cells had privileged access to nutrient, and the QS cells were not able to compete [12].

They also found that, at long times, QS cells performed better than cells that produced no matrix (referred to as EPS⁻ cells) [12]. At short times, EPS⁻ cells increased growth rate by devoting nutrients to reproduction. But at long times, EPS⁻ cells lost nutrient access to the matrix-producing QS cells. Unlike the constitutive matrix-producing cells, as the EPS⁻ cells produced no matrix, they were not able to regain the access to nutrient even after QS cells stopped producing matrix. Thus, cells employing QS have been shown to have a competitive advantage over bacteria of a fixed matrix bias. However, this advantage is only manifest at long time scales against EPS⁻ cells, and at short time scales against matrix-producing cells [12].

1.5 Simulation Framework

1.5.1 Agent-Based Modeling

The simulations for this project were performed using Agent-Based Modeling (ABM), a simulation framework that is used widely for academic research in ecology, epidemiology, and the social sciences. It is also used in commercial and governmental contexts such as business analytics, supply chain management, and military planning [13].

ABM involves representing the system of interest as a collection of autonomous actors (in our case, bacterial cells), which have well-defined behaviors and interact with one another or with the environment [13]. The environment itself can be encoded as a set of variables for the simulation. The environment can also evolve with certain dynamics independent of the agents. For example, the environments in our simulations are solutes such as nutrients used by the bacteria.

The benefit of ABM is that global dynamics emerge from many small local interactions. Only local rules are determined and communicated to the program, but one can then study the emergent global interactions. For example, as shown in Fig. 1.4, sociologists were able to model people's response to a fire in a room with a single fire escape, and found, using ABMs, the counterintuitive result that placing a column near the escape reduced risk of injury and increased escape rate [14].

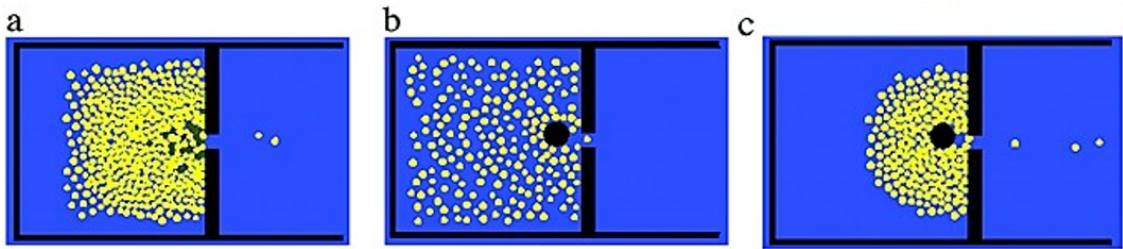


Figure 1.4: Fire escape agent-based simulation. People are represented by circles; green circles being injured people. Simulations assume 200 people in a room. (a) No column. (b) With column, after 10 s. (c) With column, after 20 s. In the absence of the column, 44 people escape and 5 are injured after 45 s; with the column, 72 people escape and no one is injured after 45 s. Figure reproduced from [14].

As seen in the example of Fig. 1.4, one of the features of ABM is the representation of spatial structure. In particular, topological details have major implications for emergent behavior, and the case shown in Fig. 1.4 is a perfect example. In our case, spatial structure is important as interactions among bacteria and interactions with the environment are often dictated by the spatial arrangement of cells. For example, one of the attributes we investigate is nutrient availability, where we incorporate a diffusing solute (to model nutrients such as O_2) into the model. The solute concentration varies by location in the simulation domain. In such a case, spatial structure largely dictates the dynamics of the bacteria such as growth rate.

1.5.2 ABM for Biofilm Modeling

So why would ABM be more useful for modeling biofilms than continuum models? We could set up differential equations for physical observables, such as the number of bacterial cells, and solve these equations analytically or numerically. However, we would not be able to explain the requirement for simple cooperative behaviors. For example, Nadell et al. (2010) demonstrate in their work that spatial structures of populations are critical for explaining the evolution of simple cooperative phenotypes. This is

because cooperative cell-lines are often subject to exploitation by rapidly growing, non-cooperative cell lines, or cheaters. The cheaters exploit the public good without contributing toward it. However, for certain spatial arrangements and preferential behaviors of cooperative cells, they may prevail [15].

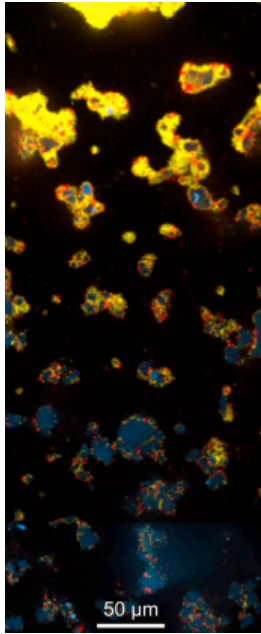


Figure 1.5: Individual cells and population structure in a static culture of *Vibrio cholerae* growing on solid chitin (shown in blue), a polymer that *V. cholerae* consumes. This picture shows the presence of cheaters (in red) growing among producer cells (in yellow) that produce the enzyme chitinase to digest the chitin. In this case, due to spatial segregation, the producer cells outcompete the cheaters. Figure reproduced from [16].

Thus, based on previous work, we believe that spatial structure and the presence of different kinds of bacteria in different arrangements are crucial to the evolution of bacteria. This is especially true when we consider a diffusive nutrient, as nutrient availability in space is extremely important.

1.5.3 Nanoverse

For this project, we used an ABM framework known as Nanoverse that was created by Dr. David Borenstein. The key feature of Nanoverse is that it allows the user to provide details of the model in terms of a simple configuration file rather than as a set of logical steps. The program parses the file and performs the simulation accordingly [13].

The Nanoverse runtime consists of a network of loosely coupled components. The

primary subsystems of the runtime are a collection of “layers” and a discrete event scheduler. The layers encapsulate information regarding the agents and the environment, such as spatial location. The scheduler encompasses all scheduling information. For processes to occur, events are added to the scheduling state with a relative waiting time, which are then performed by the scheduler in order, and subsequently removed from the scheduling state. The spatial organisation in the layers is such that information regarding elements of a layer is only available to elements in its vicinity. Thus, the agents are ignorant of the global state of the simulation [13], as would be expected in real-life situations [15].

Since the user only provides initial conditions for the simulation, events are added to the scheduling state following events run by the simulation. As soon as these events occur, the agents that have specified a reaction to particular conditions are informed, and their reactions are added to the scheduling state. The simulation thus continues until the schedule is empty, or until a terminal event is reached (such as the agent reaching a boundary) [13].

Chapter 2

Methodology

2.1 Pairwise Competitions

In this investigation, we compared bacteria of different matrix production strategies and the competitive advantage that the strategy affords in a limited nutrient environment. To evaluate the competitive advantage of strategies, we performed pairwise competitions between the bacteria of different strategies. We started the simulation with an equal number of cells of each strategy, placed in equivalent initial conditions. We then allowed the simulation to run until either of two specified halt conditions. The first halt condition for our simulations was an occupancy of 50% of the sites (that is, if 50% of the sites were filled with matrix or with bacterial cells of either strategy, the simulation would stop). The other halt condition was any one bacterial cell reaching the top boundary of the simulation domain (explained in detail below). This can be viewed as similar to the game Tetris, where the game stops when a block reaches the top of the playing field.

To evaluate the competitive advantage of the strategies, we looked at the number of cells occupied by each strategy at the end of the simulation. We ignored the matrix in our evaluations, as we considered the matrix produced by the two strategies to be identical (and they will be treated and denoted as being identical in this investigation).

2.2 Geometry of Simulations

The simulations were performed on a square lattice geometry in two dimensions. The shape of the complete simulation domain is a rectangle with a length of 128 squares, and a height of 256 squares. Each square in the lattice can either be unoccupied, or be occupied by a bacterial cell or equivalent volume of matrix¹. Each square has four neighbors. A zoomed-in snippet of the simulation domain (of length 10 and height 18) can be seen in Fig. 2.1.

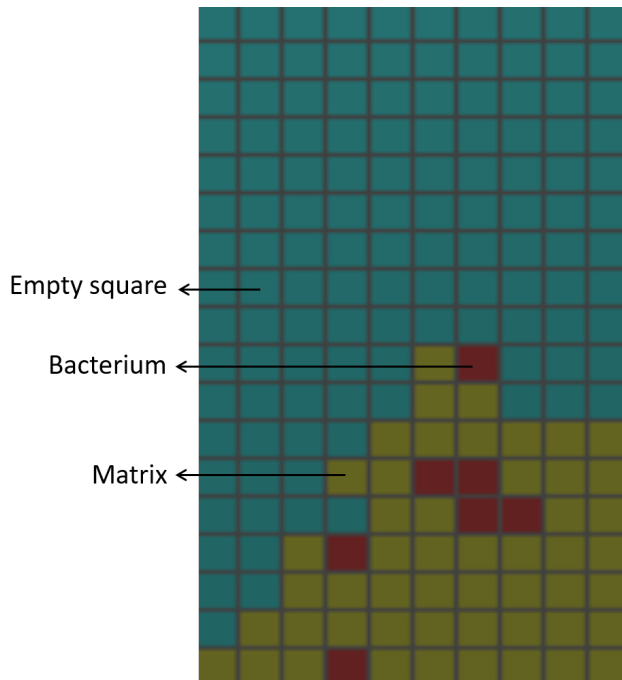


Figure 2.1: A zoomed-in snippet of a snapshot of the simulation. A sample of the simulation domain can be seen. An unoccupied square is colored cyan, a square with a bacterial cell in it is colored red, and a square filled with extracellular matrix is colored yellow.

2.3 Initial Placement of Bacteria

At the start of the simulation, the bacterial cells of two different strategies were placed randomly at the bottom of the simulation domain. 64 cells of each strategy were placed randomly at the bottom row of cells, thus filling the entire bottom layer (see Fig. 2.2).

¹Equivalent volume means an equivalent number of squares on the lattice.

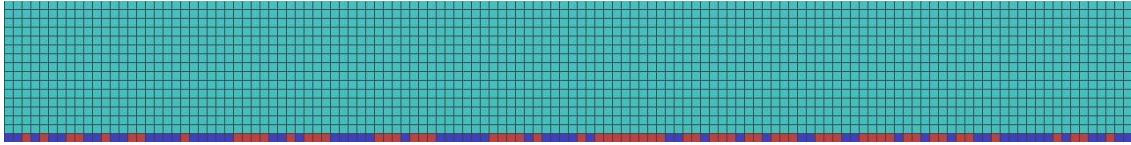


Figure 2.2: A zoomed-in snippet of the bottom of the simulation domain at initialization. The two colors (red and blue) signify the two different strategies.

We repeated our simulations with comparable numbers of cells at the beginning of the simulation, and found that our results did not vary significantly (compare Fig. 3.2 and Fig. B.6). We also tried to distribute the cells homogeneously (rather than the random distribution in Fig. 2.2). We similarly did not find any significant difference, and the random distribution was chosen as we expect distribution of bacteria in nature to be random and heterogenous.

2.4 Influx of Nutrient

A constant positive flux of nutrient was introduced to the simulation domain from the top boundary. Though our results hold for all diffusive nutrients with a source far from the biofilm, we will refer to the nutrient in our simulations as Oxygen (O_2). O_2 is used by many bacteria and a great deal of literature exists regarding the role of O_2 in biofilms [17], but many other metabolites such as nitrite, nitrate, ammonium, pH, sulfide, and methane can be equally important and lead to spatial heterogeneities in biofilm chemistry and biology [18].

In the simulation environment, O_2 diffuses in from the top boundary toward the bacterial cells. The bacterial cells consume O_2 at a linear rate and act as sinks of O_2 . Thus, at steady state, the amount of O_2 consumed globally by the cells (δ_{consumed}) is the same as the constant flux of O_2 into the whole system (δ_{in})

$$\begin{aligned} \frac{d[O_2]}{dt} &= \delta_{\text{in}} - \delta_{\text{consumed}} \\ \frac{d[O_2]}{dt} &= 0 \implies \delta_{\text{consumed}} = \delta_{\text{in}} \end{aligned}$$

The complete simulation domain along with the influx of O_2 represented by arrows (indicating the direction of flux of O_2) can be seen in a snapshot of a simulation in Fig. 2.3. As indicated in Fig. 2.3, the influx of O_2 was invariant of the column number. That is, the influx of O_2 was horizontally symmetric in the simulation domain.

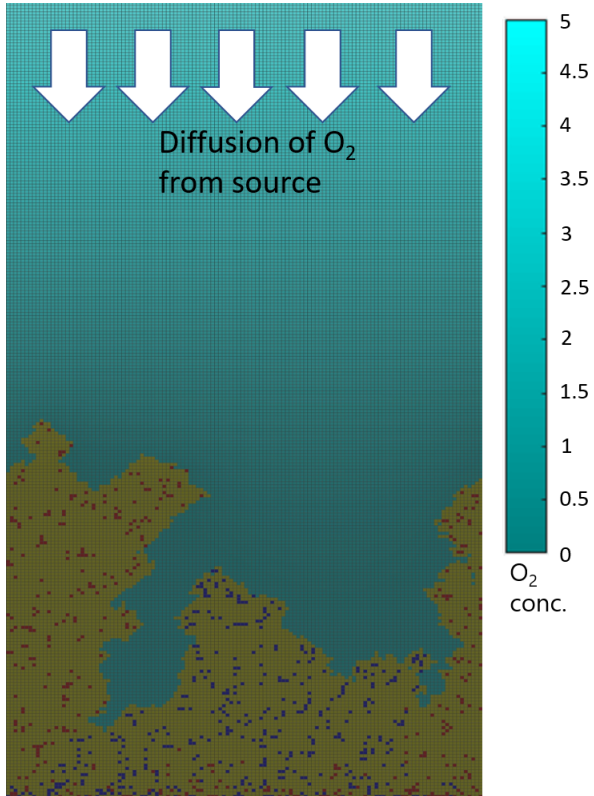


Figure 2.3: A snapshot of a simulation. The red and blue squares indicate bacterial cells of different fixed-rate strategies. The yellow squares indicate squares occupied by matrix. The white arrows indicate the direction of influx of O_2 into the simulation domain. The cyan squares of different shades indicate unoccupied squares. The shade of cyan indicates the average concentration of O_2 in the square (given by the color bar to the right)

2.5 Boundary Conditions

The geometry has periodic boundary conditions in the horizontal axis. Thus, a bacterial cell that passes through the right boundary will enter in the left end of the simulation at the same height. This can be viewed as being like another arcade game, Pacman. Similarly, the concentration of O_2 at the right end of the simulation is the same as the concentration at the left end of the simulation domain for the same vertical coordinate. By this boundary condition, we wish to simulate a large horizontal domain in which the biofilm can grow. Periodic boundary conditions eliminate any

exceptional behavior of the biofilm at the horizontal boundaries that would not be expected away from the boundary. This is because our simulations treat the sites at the boundary just like any other site in the domain. The neighboring squares for the squares at either horizontal boundary are thus located at the other end of the simulation domain.

For O_2 , the boundary conditions at the top and bottom of the simulation domain are reflecting boundary conditions. Reflecting boundary conditions are also known as zero-flux boundary conditions in diffusive systems and are specific examples of Neumann boundary conditions. Thus, no O_2 enters or leaves the system from the top or the bottom boundary. To maintain the constant influx of O_2 described in §2.4, we designate the top row of squares as oxygen-producing squares that produce O_2 at a constant rate.

For the bacteria, the bottom boundary acts as a hard boundary. Thus, bacteria cannot be shoved into the bottom of the simulation domain. The top of the simulation domain acts as a halting boundary condition. Any bacteria that reach the top of the simulation domain cause the simulation to halt immediately.

2.6 Reaction Diffusion Equation

In general, the concentration of oxygen, $[O_2]$, at any site is described by the following differential equation [19]:

$$\frac{\partial [O_2]}{\partial t} = D_{O_2} \nabla^2 [O_2] - \mu [O_2] + \delta_d(\vec{x}) \rho_{O_2}$$

where D_{O_2} is the diffusion constant for O_2 , μ describes the rate of consumption of O_2 , $\delta_d(x)$ is a 2-dimensional Dirac delta function which is nonzero at the center of each oxygen-producing square, and ρ_{O_2} is the rate of production of O_2 . This reaction-diffusion process is solved for the lattice. The discrete spacing to solve the equation is taken to be equal to a square, which is the size of the cell. For technical notes regarding the solution of the reaction-diffusion equation, please refer to §A.2.

2.7 Reproduction and Production of Matrix

The bacterial cells can perform two actions: reproduction and production of matrix. Both reproduction and the production of matrix are stochastic processes. At every time step, the probability of reproduction by a cell is calculated as per the formula $r_r[O_2]$, where r_r is the coefficient of reproduction and $[O_2]$ is the local concentration of O_2 at the site of the cell. A random number from a uniform distribution between 0 and 1 is then generated, and if the random number is less than the probability value for reproduction, the cell produces a copy of itself².

Similarly, the probability of matrix production is calculated as per the formula $\frac{1}{2}r_m[O_2]$ where r_m is the coefficient of matrix production, and a random number is chosen to decide if two unit volumes of matrix will be produced. The simulation was configured such that two unit volumes of matrix were produced at half the rate of production of matrix. This algorithm replicates the structure of biofilm observed in experiments better than producing one unit volume of matrix at the rate of matrix production.

It must be noted here that the process of matrix production and reproduction are independent: in the same time step, a cell might reproduce and produce two units of matrix. The probability of such an event occurring is the product of the probabilities of either event occurring, that is $\frac{1}{2}r_r r_m [O_2]^2$. Similarly, a timestep may feature neither of these actions with a probability of $(1 - r_r[O_2])(1 - \frac{1}{2}r_m[O_2])$.

2.8 Shoving Algorithm

Our simulation does not incorporate cell death, and no cells or matrix are removed from the simulation. With matrix production and reproduction, the volume of biomass increases and new lattice sites need to be occupied. As the cells that are reproducing

²If the calculated probability is greater than one, the simulation is immediately halted.

or producing matrix may be in the interior of the biofilm, the cells must shove biomass toward the edge of the biofilm. The algorithm for shoving is detailed in steps below, and the cumulative result of all steps are depicted in Fig. §2.4. Steps 1-5 are common for both matrix production and reproduction (and both panels of Fig. §2.4). All distances are measured by l_1 distance, also known as Manhattan distance.

1. The closest vacant sites to the parent site (the site reproducing or producing matrix) are identified.
2. One of the closest vacant sites is chosen randomly.
3. The shortest paths to the chosen vacant site are identified. Paths are sequences of distinct lattice sites. All lattice sites in a path must be neighbors to the lattice sites before or after them in the path. The last lattice site in the path to a vacant site is the vacant site itself.
4. One of the shortest paths is chosen randomly.
5. all the occupants of the lattice sites in the path occupy the next lattice site in the path. Thus, the second lattice site of the path, after the active site, is now unoccupied. This lattice site will be called the daughter site.
6. If the action is reproduction, a copy of the cell reproducing is placed in the daughter site (Panel a of Fig. §2.4).
7. If the action is matrix production, half of the times the matrix will occupy the daughter site (and the cell will occupy the matrix site). The other half of the times, the cell will occupy the daughter site, and the matrix will occupy the parent site. The choice between the two alternatives is made randomly.

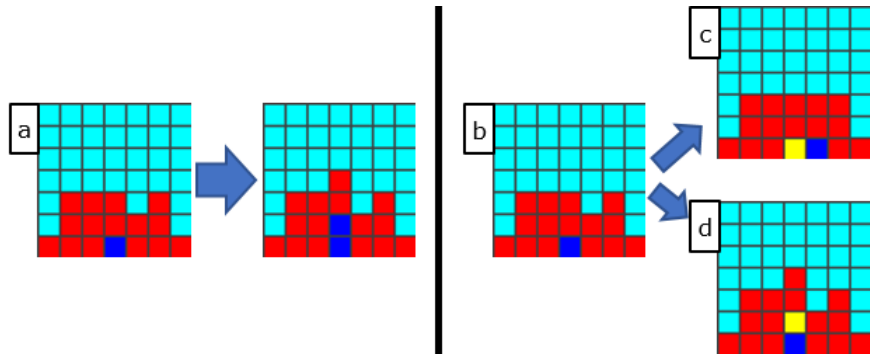


Figure 2.4: Demonstration of the shoving algorithm used for matrix production and reproduction. These are snapshots of simulations before and after both processes. The blue cell here is the active cell, while the red squares are not active. The cyan squares are unoccupied. *Panel a* depicts reproduction. *Panels b, c and d* depict matrix production, where *panels c and d* depict the two possible cases of matrix production.

The algorithm for shoving is extremely important as it establishes the spatial dynamics discussed in §1.5.2. Our algorithm results in a compact biofilm (see Fig. 3.1) as is witnessed in nature. This is because the nearest vacant sites are occupied first. It also causes a homogeneous distribution of matrix and bacterial cells because the cells are pushed away from the parent site and toward the edge of the biofilm only half of the time. The other half of the time, the cells stay at the parent site.

2.9 Discussion of Parameters

Each of the processes in our simulation, such as diffusion of O₂ and matrix production, can be quantitatively described. The parameters used to describe the processes quantitatively are extremely important. We used values similar to the experimental values for commonly studied species of bacteria.

There were two time scales that were relevant in our simulations. We assumed that the time scale of reproduction is much much longer than that of equilibration for the reaction-diffusion equation. We shall first describe the parameters for processes in the time scale of reproduction.

Property	Value used	Exp. Value	Source of value
Time	1 time step ≈ 1 hour	0.71 to 1.13 hours	Doubling time of <i>Escherichia coli</i> in aerobic M9 minimal media [20]
Volume of cell	1 square in lattice ≈ 1 μm^3	0.44-1.79 μm^3	Cells of several different sizes were obtained from stationary-phase cultures of <i>E. coli</i> B/rA grown overnight at 37 °C in a shaker water bath in nutrient broth or M9-glucose (10 g/liter) medium [21]
Aerobic biomass production rate	0/hour	0.18-0.90/hour	Growth rate of different strains of <i>E. coli</i> in anaerobic M9 minimal media [20]
Cost of reproduction relative to matrix production (for equal volumes)	14	13.48	Experiments conducted by Jing Yan, Princeton University

Table 2.1: Parameters for processes in the time scale of reproduction. These parameters were used for all simulations discussed in this investigation.

The parameters for processes in the time scale of equilibration for the reaction-diffusion equation are described below. As the time scale is not defined, the parameters should be considered relative to each other for some unit of time. The length scale is 1 μm .

Property	Value used	Exp. Value	Source of value
Diffusion Constant of O ₂	0.005	$2.20 \times 10^5 \text{ cm}^2/\text{s}$	Diffusion of O ₂ in water at 25 °C [22]
Typical concentration of O ₂	0-5	0.258 mM	Solubility of O ₂ in water at 25 °C and pressure of 760 mm of Hg [23]
Rate of consumption of O ₂	Coefficient of 0.01 $\equiv 2.58 \times 10^{-12} \mu\text{m}$ of O ₂ /cell/s (for typical concentration of O ₂ from [23])	$1.556 \times 10^{-12} \mu\text{m}$ of O ₂ /cell/s	Respiration rates of bath cultures of <i>Escherichia coli</i> grown in minimal media supplemented with various carbon sources which supported growth at specific growth rates from 0.2 to 1.3/h [24]
Net flux of O ₂	0.128	Depends on O ₂ source	

Table 2.2: Parameters for processes in the time scale of equilibration for the reaction-diffusion equation. These parameters were used for all simulations discussed in this investigation.

Chapter 3

Optimizing Matrix Production without Quorum Sensing

Our first task of investigation was to find the optimal matrix bias for bacterial cells that do not perform QS in biofilms. We sought to find this value by comparing several matrix production strategies with each other, two at a time.

3.1 Reproduction and Matrix Production

In the configurations for our simulations, the coefficient of reproduction, r_r , and the coefficient of matrix production, r_m , (discussed in §2.7) are related by the equation:

$$r_r + \beta r_m = 1$$

where β is the cost of matrix production relative to reproduction (per unit volume). Both coefficients refer to the production of one unit volume (equal to one square in the lattice of the simulation) per unit time per unit concentration (of O₂). As producing matrix is cheaper, per unit volume, we expect $\beta < 1$. Experimentally, we find that $\beta = 1/13.48$ (see §2.9). For our simulations, we use the value $\beta = 1/14$.

Thus, r_r and βr_m are the proportions of resources devoted by each cell to reproduction and matrix production respectively. For a cell that did not produce matrix, r_m would be 0. The matrix bias of any strategy is just βr_m . For cells that do not utilize QS (which are the focus in this chapter), r_r and r_m do not change with time. Due to the constancy of these coefficients, these strategies will be referred to as *fixed strategies*.

3.2 Results and Discussion

3.2.1 Pair-wise Competitions

We performed pair-wise competitions between pairs of fixed strategies with matrix biases ranging from 0 to 0.9 (in increments of 0.1). An example of snapshots at different time points in an example of simulations of pairwise competitions can be seen in Fig. 3.1.

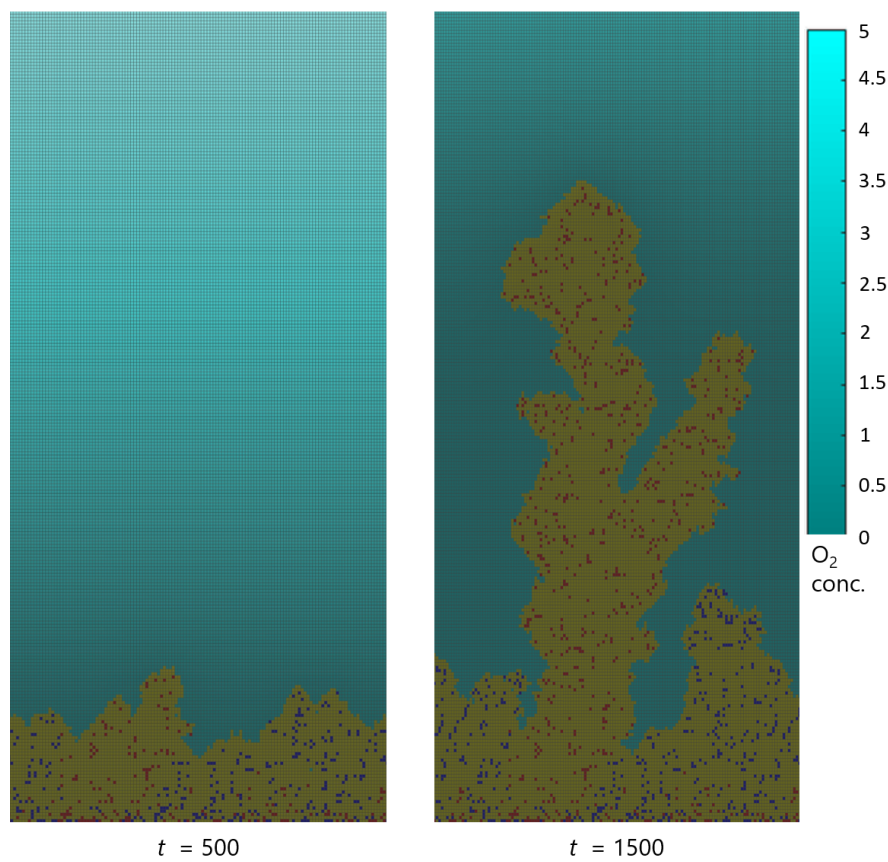


Figure 3.1: Snapshots of a simulation of pairwise competition between two fixed strategies (differentiated by color). Red cells have a matrix bias of 0.6 while blue cells have a matrix bias of 0.5. The left snapshot is after 500 timesteps and the right snapshot is after 1500 timesteps. Yellow squares are occupied by matrix and cyan squares are unoccupied. Shades of cyan squares indicate the O_2 concentration at the sites.

To evaluate the competitive advantage of two strategies, say A and B , we looked at the ratio, $n(A)/n(B)$, where $n(A)$ is the number of cells of strategy A , and B is the number of cells of strategy B . As each simulation has many stochastic processes in it (detailed in §2.3, §2.7 and §2.8), no two simulations are identical. We repeated many simulations for the same pairs of matrix bias values. The average results from all simulations can be seen in the heatmap in Fig. 3.2. Each point in the heatmap indicates the log of the ratio $n(A)/n(B)$ at the end of the simulation, averaged over all the simulations performed for that pair of values.

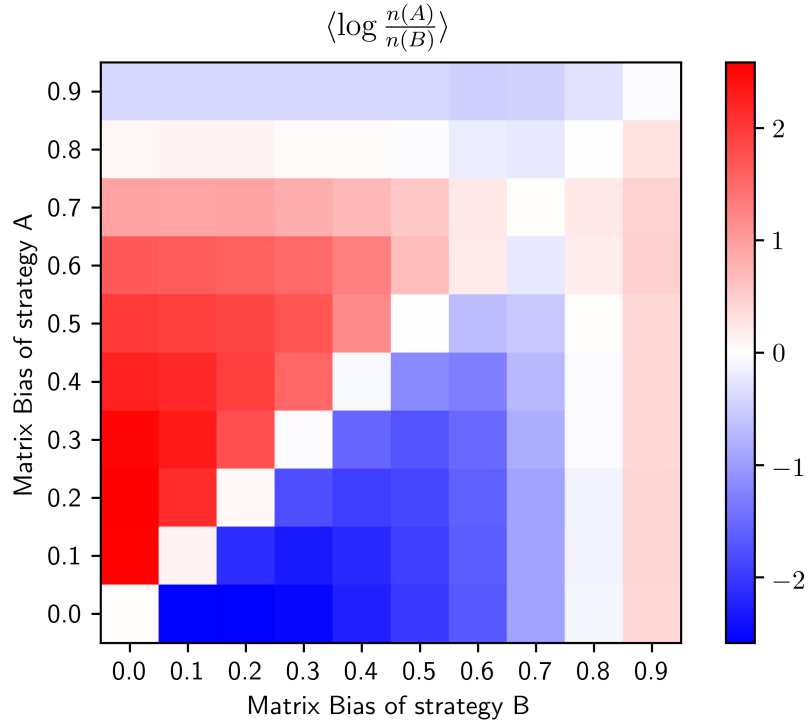


Figure 3.2: Logarithm of the final ratio of number of strategy A cells (indicated by row number) to number of strategy B cells (indicated by column number), averaged over many simulations.

Thus, we find that for our parameters, the optimal matrix bias is 0.7. That is, at the end of the simulation, bacteria with a matrix bias of 0.7 will have a higher cell

count than bacteria with other matrix bias values. The data in the heatmap above is anti-symmetric, that is $\langle \log \frac{n(A)}{n(B)} \rangle = -\langle \log \frac{n(B)}{n(A)} \rangle$. For example, the value for 0.8 as the matrix bias of strategy A and 0.6 as the matrix bias of strategy B, is exactly the negative of the value for 0.6 as the matrix bias of strategy A and 0.8 as the matrix bias of strategy B. Thus, the heatmap above has 55 unique values plotted. The number of simulations performed to obtain each of the values in Fig. 3.2 is given in Fig. 3.3.

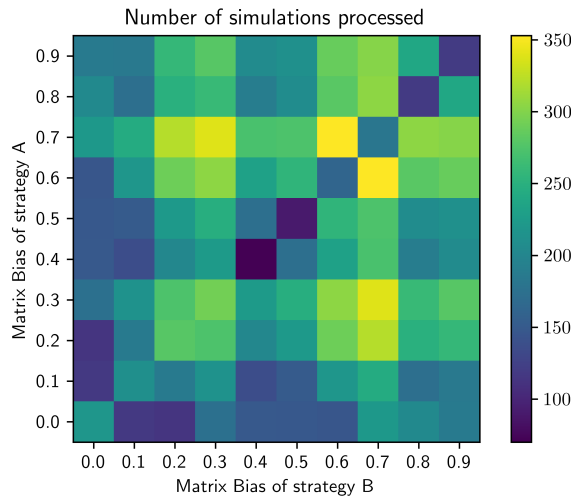


Figure 3.3: The number of simulations completed for each pair of strategies to generate the values for Fig. 3.2.

Thus, for each pair of strategies, there is a distribution of values of the log of the ratio. The standard deviation of each of the distributions is shown in Fig. 3.4.

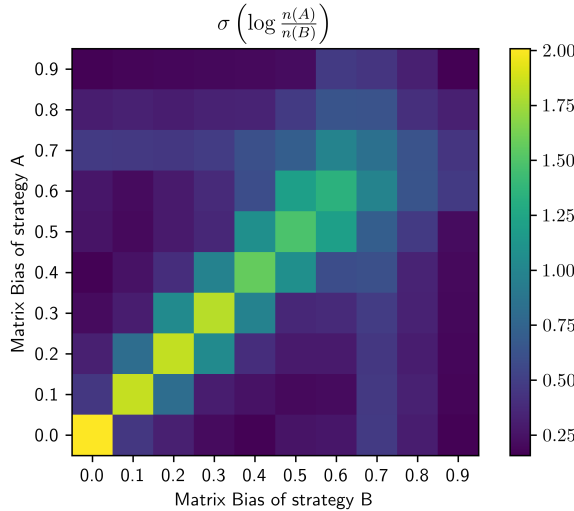


Figure 3.4: Standard deviation of the distribution of logarithms of final ratios for each pair of strategies.

The standard deviation is highest in distributions where the matrix bias is the

same for both strategies. This is because when the strategies are identical, either strategy is equally likely to gain a competitive advantage. Thus, the mean was near 0 ($\mu = 0.02$ as seen in Fig. 3.2) but the standard deviation was high ($\sigma = 2.01$). Other plots relevant to competitions between fixed strategies, including analyses of contribution toward matrix production by each strategy, can be found in §B.

3.2.2 Time Dependence

The results shown above are specific to the parameters discussed. As would be expected, for a higher cost of matrix, a lower matrix bias is optimal. Similarly, for a higher diffusion coefficient (which might be the case if a different nutrient were chosen), a lower matrix bias is optimal as the difference between nutrient concentrations in the interior and at the edge of the biofilm is low. Generally, conditions that foster competition for access to nutrient favor a higher matrix bias. While there are many parameters that could be changed, we would like to highlight the dependence of the results on the time for which the simulation is run¹. The ratio $n(A)/n(B)$ was calculated at different time points of the simulations. The average ratios can be seen in the heatmap in Fig. 3.2. Each point in the heatmap indicates the log of the ratio $n(A)/n(B)$ after the specified number of timesteps, averaged over all the simulations performed for that pair of values.

¹It serves to remind the reader that for the simulations that provided the data used to generate Fig. 3.2, there was no uniformity in the number of timesteps. Rather, the simulations halted at different time points. The average number of timesteps for simulations with each set of matrix bias values can be seen in Fig. B.4.

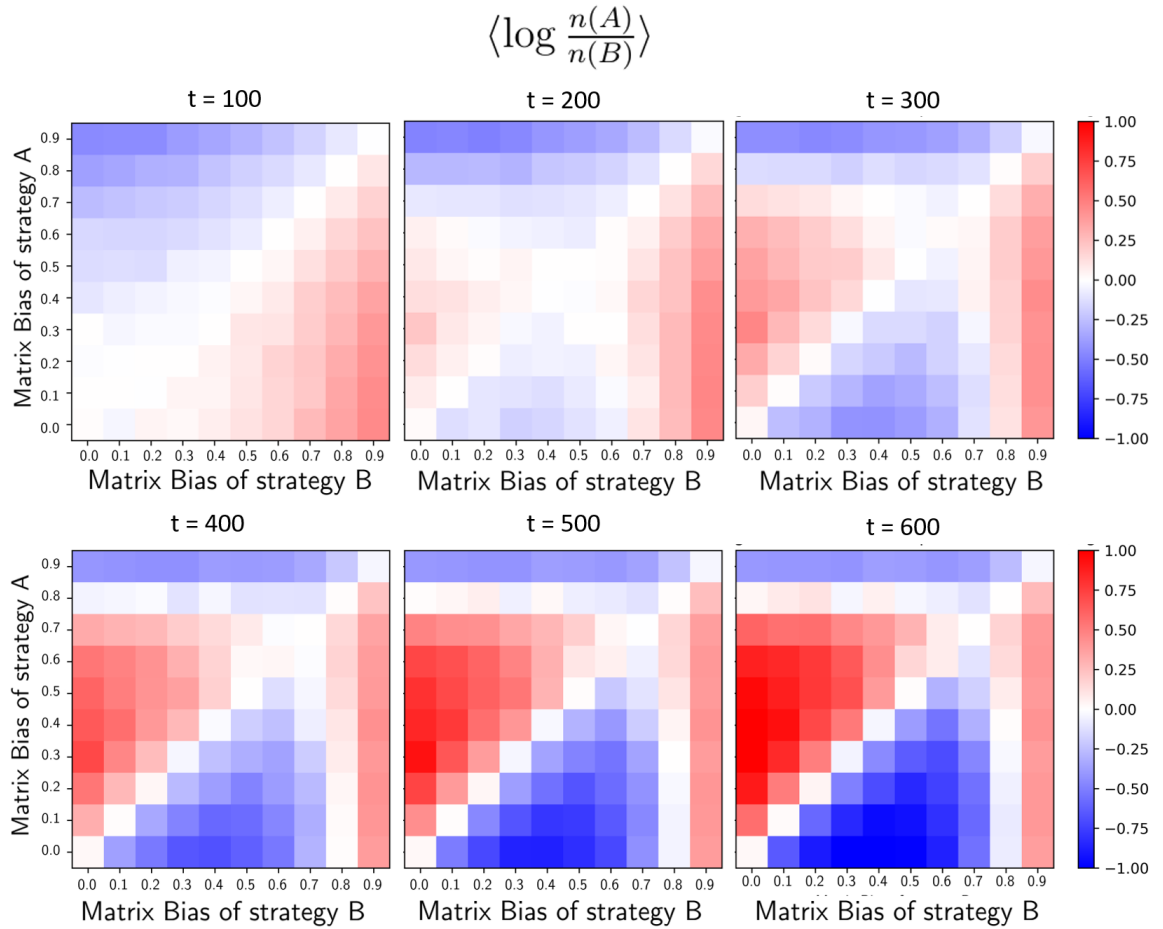


Figure 3.5: The progression of the mean of the log of the ratio of numbers of fixed strategies over time. The row number in all plots indicates the matrix bias of strategy A, and the column number indicates matrix bias of strategy B. The matrix biases for both strategies range from 0.1 to 0.9 in increments of 0.1. The number of time points from the start of the simulation is indicated above each plot.

As can be seen in Fig. 3.5, at short time scales a low matrix bias results in a higher number of cells. This is because the cells do not divert resources to matrix production and the growth rate is high. However, over time the competitive advantage due to matrix production becomes evident, and the cells with a higher matrix bias gain more access to nutrient, at the expense of cells with a lower matrix bias. The higher

availability of nutrient results in a higher rate of reproduction (as rate of reproduction is linear to O_2 availability), and subsequently in a higher number of cells produced. Over time, cells with a higher matrix bias start gaining a competitive advantage. These are exactly the results that Nadell et al. obtained for their simulations.

Extrapolating from our results, we can predict that for a large enough simulation domain, the optimal matrix bias would be 0.9 (or even higher if the increments of matrix biases are smaller). However, it must be noted that in real biological situations, biofilms do not grow indefinitely, but disperse after some time. Dispersal in a biofilm occurs at different times for different species, and is also dependent on environmental conditions [25]. Dispersal is regulated by different environmental cues and inter- and intracellular signals [25]. Thus, the optimal matrix bias value found in nature will be different for different species and even under different circumstances. For example, for *E. coli*, the proportion of cells by mass in a biofilm is 15% (and the remaining 85% is matrix). If the allocation of resources is roughly proportional to the mass, the matrix bias for *E. coli* is around 0.85.

3.2.3 Margins of Advantage

As seen in Fig. 3.2, a matrix bias of 0.7 will have a higher cell count in pairwise competitions with other matrix bias values for our simulation configuration. However, while a matrix bias of 0.2 will not have a higher cell count than matrix bias values between 0.3 and 0.7, when it does have a higher cell count (as against matrix biases of 0 and 0.1), the ratio of cell counts is very large. This can also be seen in the comparison between fixed strategies of matrix bias 0.2 and 0.7 in Fig. 3.6.

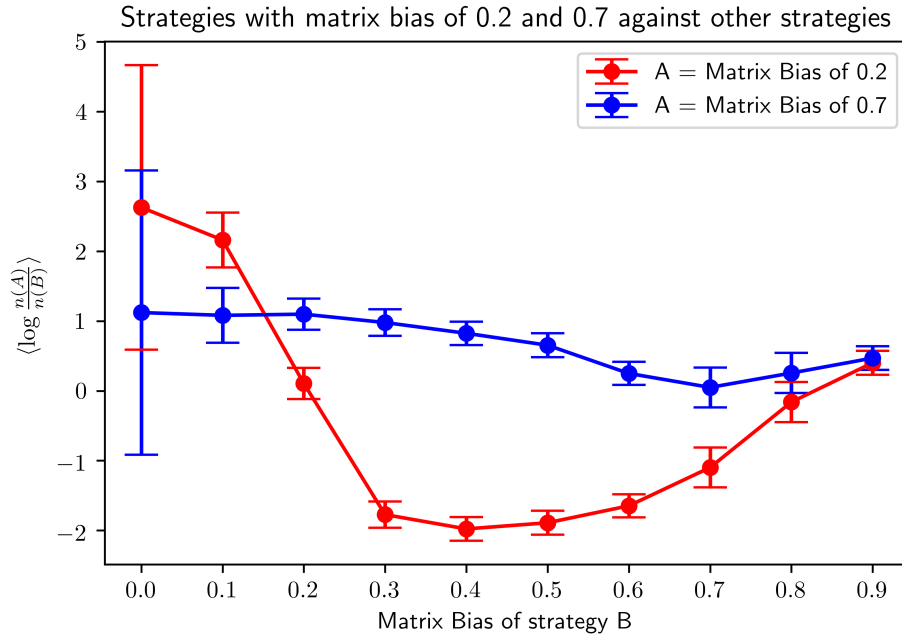


Figure 3.6: Mean of the logarithm of the ratio of number of cells of bacteria with matrix bias 0.2 and 0.7 (labeled as strategy A) in simulations with bacteria with other matrix biases (labeled as strategy B). The error bars indicate the standard deviation in the logarithm of the ratio.

This can also be seen in snapshots of the simulation domain at the end of the simulation for bacteria with matrix biases 0.2 and 0.7 in pairwise competitions with bacteria with a matrix bias of 0.1 (see Fig. 3.7). The snapshots show that while both matrix production strategies gained the competitive advantage against bacteria of matrix bias of 0.1, bacteria of matrix bias of 0.2 have a significantly higher cell count. This is because producing less matrix allows the bacteria to increase its growth rate by allocating all its resources to reproduction. Both matrix production strategies gained a competitive advantage against their competition, and after gaining exclusive access to nutrient, the proportion of resources dedicated to reproduction determined their final cell count.

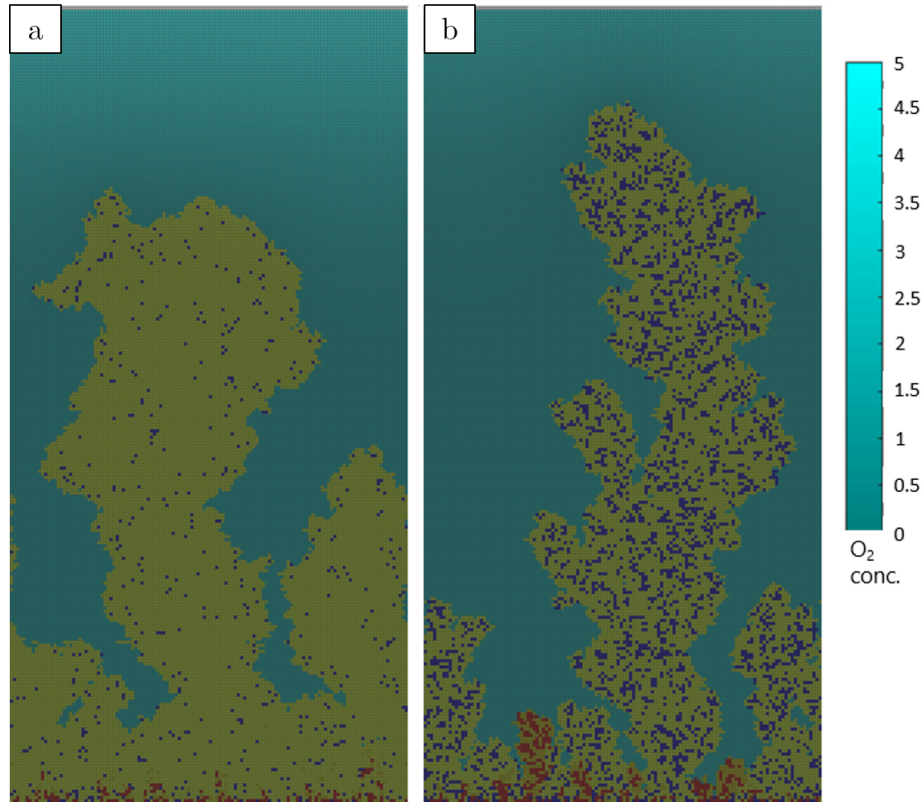


Figure 3.7: Snapshots of the simulation domain at the end of simulations for bacteria with matrix biases 0.7 (*panel a*) and 0.2 (*panel b*) in pairwise competitions with bacteria with a matrix bias of 0.1 (labeled red). Higher matrix bias cells in both cases are labeled blue. Yellow squares are occupied by matrix, and cyan squares are unoccupied with an O_2 concentration indicated by the shade. In panel a, bacteria with matrix bias of 0.7 occupy 331 cells, while bacteria with matrix bias of 0.1 occupy 120 cells. In panel b, bacteria with matrix bias of 0.2 occupy 2935 squares, while bacteria with matrix bias of 0.1 occupy 321 squares

Thus, matrix production is beneficial in gaining access to a nutrient only in the presence of competition. After limiting access to nutrient to the competition, bacteria should switch allocation of resources to reproduction. We wondered if bacteria could use communication to implement such a switch-like behavior. To this end, we incorporated QS into our simulation configuration.

Chapter 4

The Role of Quorum Sensing

4.1 Constitutive Autoinducer Production

To incorporate QS, we introduced a new solute in Nanoverse. This solute, autoinducer (AI), is the chemical signaling molecule used by bacteria for QS. The sources of AI are the cells, which produce AI at a constant rate. The boundary conditions for AI are periodic boundary conditions on the left and right boundaries, reflecting (zero-flux) boundary conditions at the bottom boundary, and an absorbing boundary condition at the top boundary. An absorbing boundary condition holds the concentration at that boundary to always be 0. This is also known as a Dirichlet boundary condition (with a specified value of 0). Thus, the reaction diffusion equation is given by,

$$\frac{\partial[\text{AI}]}{\partial t} = D_{\text{AI}} \nabla^2 [\text{AI}] + \delta_a(\vec{x}) \eta_{\text{AI}}$$

with the condition that $[\text{AI}] = 0, \forall t$ at the top boundary; D_{AI} is the diffusion constant for AI, $\delta_a(\vec{x})$ is a 2-dimensional Dirac delta function which is nonzero at the center of each AI producing cell, and η_{AI} is the rate of production of AI.

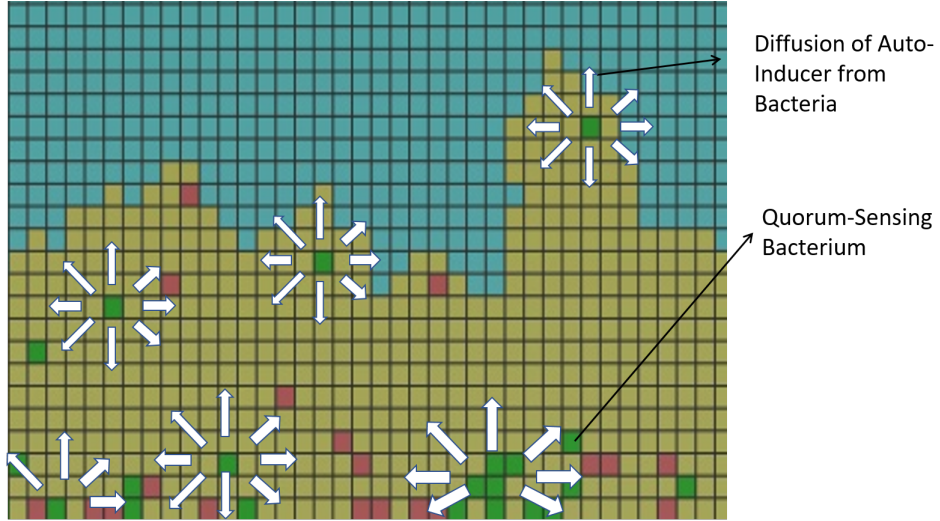


Figure 4.1: A zoomed-in snippet demonstrating the model of constitutive AI production. The green squares are occupied by QS cells that secrete AI molecules at a constant rate. The white arrows indicate the direction of diffusion of AI molecules away from their source, the QS cells. The QS cells also detect the local AI concentration. The red squares are occupied by cells that produce matrix at a fixed rate and neither produce nor detect AIs. The yellow squares are occupied by matrix, and the cyan squares are unoccupied.

4.2 Autoinducer Detection

The coefficient of reproduction, r_r , and the coefficient of matrix production, r_m , now depend on the local AI concentration. r_r is given by the following expression:

$$r_r([\text{AI}]) = O + (M - O) \frac{[\text{AI}]^n}{(K_h)^n + [\text{AI}]^n}$$

The terms of the expression are as follows:

1. n is the coefficient of cooperativity
2. O is the minimum value obtained by r_r
3. M is the maximum value obtained by r_r

4. K_h is the AI concentration at which r_r attains the value $\frac{1}{2}(O + M)$

The coefficient of matrix production, r_m , is still related to r_r by the equation:

$$r_r([\text{AI}]) + \beta r_m([\text{AI}]) = 1$$

The forms of r_r and r_m for different values of [AI] can be seen in Fig. 4.2

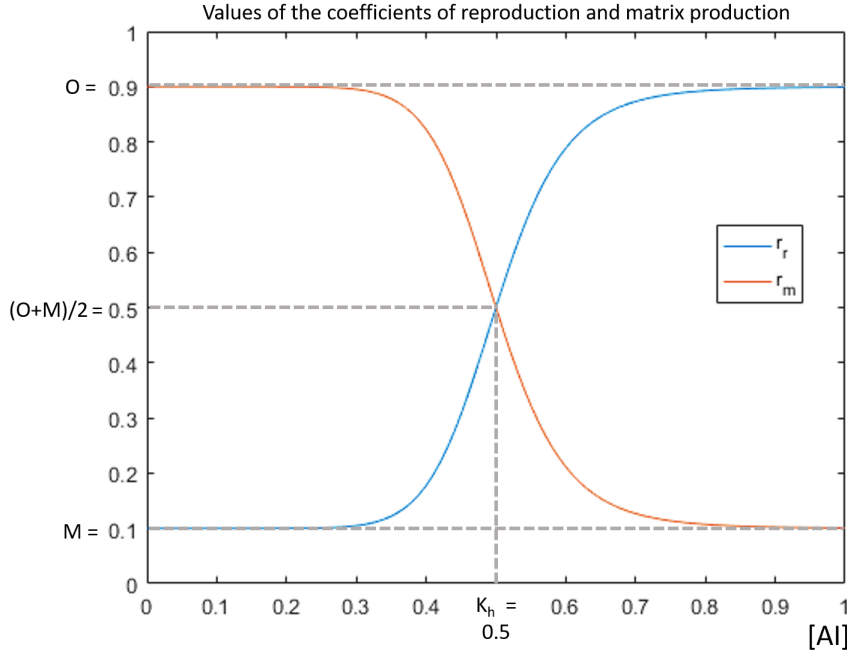


Figure 4.2: The forms of r_r and r_m for different values of [AI]. The parameters used were $n = 10$, $O = 0.1$, $M = 0.9$ and $K_h = 0.5$

These forms for r_r and r_m thus reflect the relatively switch-like behavior exhibited by many quorum-sensing bacteria. The behavior is more switch-like for higher coefficients of cooperativity, n . n indicates the cooperativity of AI molecules in initiating a change in matrix bias.

4.3 Discussion of Parameters

The production and detection of AIs can be quantitatively described in terms of many parameters. In this case, we did not seek to mimic actual QS systems, but demon-

strate that QS systems exist that perform better than all fixed strategies. Since it was relatively easy to design such a system, we believe that these parameters are not specially poised. Other sets of reasonable parameters were used, and results similar to the ones described below were obtained. The parameters used in Nanoverse to generate the results described below are as follows (for descriptions of these parameters, please refer to §4.1 and §4.2):

Property	Value used
n	10
O	0.1
M	0.9
K_h	20
η_{AI}	10^{-5}
D_{AI}	10^{-4}

Table 4.1: Parameters used to incorporate QS into the simulation. These parameters describe the production and detection of AI molecules by QS cells

All other parameters used were the same as described in §2.9.

4.4 Results and Discussion

We performed pair-wise competitions between the QS strategy described above, and fixed strategies with matrix biases ranging from 0 to 0.9 (in increments of 0.1). An example of snapshots at different time points in an example of simulations of pairwise competitions can be seen in Fig. 4.3. As seen in these snapshots, QS cells gain a competitive advantage in the first few hundred timesteps by producing mostly matrix, and switch to mostly reproduction after around 400 timesteps.

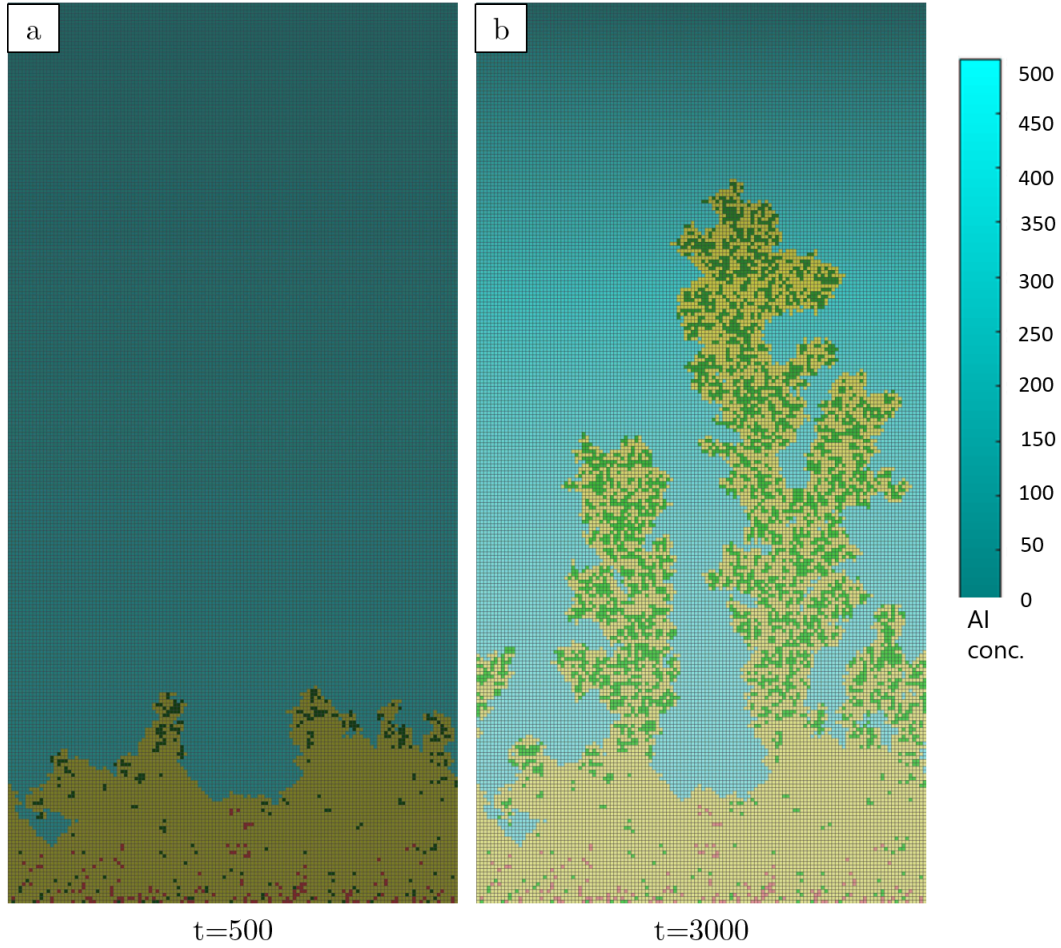


Figure 4.3: Snapshots of a simulation of pairwise competition between a constitutive AI producing QS strategy and a fixed strategy (differentiated by color). Green cells produce and detect AI while red cells have a matrix bias of 0.4. The left snapshot is after 500 timesteps and the right snapshot is after 3000 timesteps. Yellow squares are occupied by matrix and cyan squares are unoccupied. The shades of cyan squares indicate the AI concentration at the sites.

To evaluate the competitive advantage of the two strategies, we looked at the ratio, $n(\text{QS})/n(\text{Fixed})$, where $n(\text{QS})$ is the number of cells of the QS strategy, and $n(\text{Fixed})$ is the number of cells of the fixed strategy. We repeated many simulations for each fixed strategy. The average results from all simulations can be seen in the plot in

Fig. 4.4. For a comparison, the results from the competition of cells with the optimal fixed strategy, which had a matrix bias of 0.7, is also plotted. Each point in the plot indicates the log of the ratio $n(\text{QS})/n(\text{Fixed})$ at the end of the simulation, averaged over all the simulations performed for that pair of values. Over 70 simulations were performed for competitions between cells performing QS and each fixed strategy.

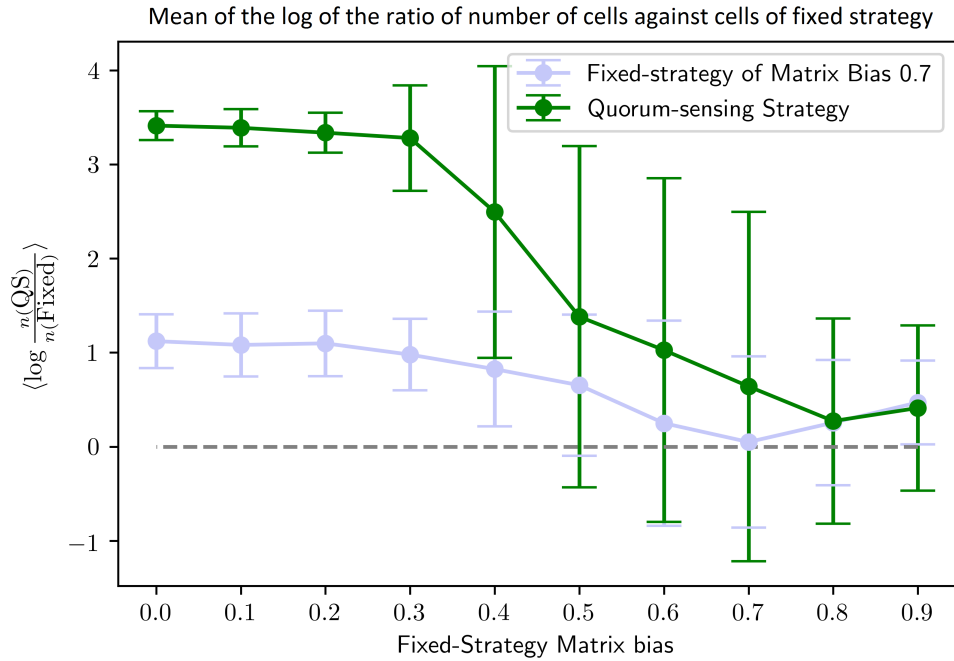


Figure 4.4: Logarithm of the final ratio of number of QS cells to number of fixed strategy cells, with a matrix bias given by the x-axis. The result is the average over many simulations. The logarithm of the final ratio of number of cells for competitions between cells with the optimal matrix bias and other fixed strategies is also plotted. The grey dashed line corresponds to a y-value of zero. All error bars are standard deviations of the values.

Thus, we found that not only do QS cells out-compete all fixed strategies on average, QS cells are also able to out-compete fixed strategy cells by a much larger margin than the optimal fixed strategy.

Chapter 5

Oxygen-dependent AI Production

5.1 Biological Motivation

In Chapter 4, we showed that QS can afford a competitive advantage in accessing a diffusive nutrient if AI production is constitutive. However, it is believed that for all quorum-sensing systems, the substrates for AI production are derived from general metabolites [26]. As these metabolites are critical for many other functions in bacteria, the composition of these metabolites in the environment of the biofilm would be reflected in the overall physiological state of the bacterium. For example, in the case of acyl-homoserine lactone (acyl-HSL) systems of many gram-negative species, the substrates for AI synthesis are S-adenosyl methionine (SAM) and acylated acyl carrier protein (acyl-ACP) [27] [28].

SAM can affect a broad array of mechanisms [29]. Produced by the one-carbon metabolism cycle, SAM is the donor for methylation of histones and other proteins, nucleic acids, and is used in phospholipid synthesis [29]. One-carbon metabolism is often followed by many other oxidative steps, and reflects the overall metabolic state of the cell, which would be dependent on nutrient availability [26].

Further, the composition of acyl-ACP will depend on the metabolic state of the cell [30]. As cells buried in the interior of a biofilm show decreased metabolic activity, Parsek et al. argue that the decreased metabolic activity could affect SAM and acyl-ACP levels and that, in turn, the levels of acyl-HSL synthesis might differ in the

interior of the biofilm compared with the metabolically active edge of the biofilm [26]. Thus, Parsek et al. argue that limited nutrient availability would affect signal gradients in the system. They present the same argument regarding the pools of acyl-ACP available for AI synthesis [26] as acyl-ACP is involved with the fatty acid biosynthesis pathway.

Parsek et al. state that the positive autoregulation of AIs in many QS systems complicates the experimental verification of this question [26]. This is because if a subpopulation of the biofilm were induced to produce AIs, the other parts of the biofilm would also be induced to produce AIs. Thus, knowing where AI production is first induced is vital to answering the question, but is experimentally very difficult to realize [26]. However, we present a theoretical argument to demonstrate that if AI production did depend on substrate availability, QS would fail due to a limited dynamic range of AI concentrations. We were motivated to seek a theoretical justification due to the following results from ABM simulations.

5.2 Methodology

The configuration was identical to the case of constitutive AI production, except that the rate of production of AI was taken to be linear to the local O_2 concentration. Thus, the reaction diffusion equation is given by

$$\frac{\partial [AI]}{\partial t} = D_{AI} \nabla^2 [AI] + \delta_a(\vec{x}) \rho_{AI} [O_2]$$

with the condition that $[AI] = 0, \forall t$ at the top boundary; D_{AI} is the diffusion constant for AI, $\delta_a(x)$ is a 2-dimensional Dirac delta function which is nonzero at the center of each AI producing cell, and ρ_{AI} is the coefficient of AI production.

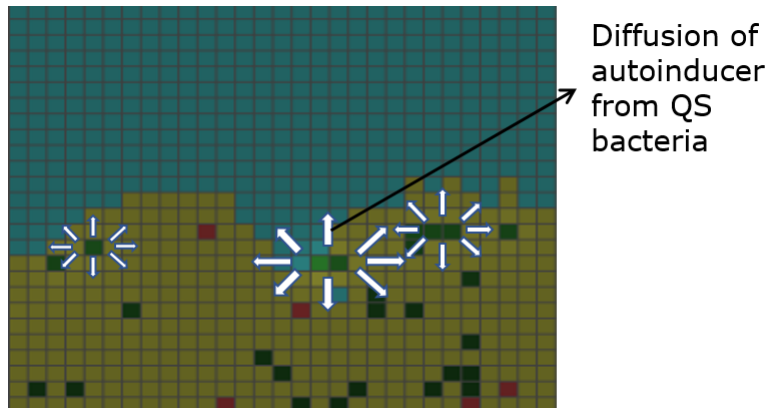


Figure 5.1: A zoomed-in snippet demonstrating the model of oxygen-dependent AI production. The green squares are occupied by QS cells that secrete AI molecules at a constant rate. The white arrows indicate the direction of diffusion of AI molecules away from their source, the QS cells. The QS cells also detect the local AI concentration. The red squares are occupied by cells that produce matrix at a fixed rate and neither produce nor detect AIs. The yellow squares are occupied by matrix, and the cyan squares are unoccupied.

5.3 Discussion of Parameters

The results below discuss AI production with a coefficient of AI production, ρ_{AI} , of 1000. All other parameters are the same as described in §4.3. It must be noted that simulations with many other sets of parameters, including the parameters discussed in §4.3, were also investigated. However, the conclusions that we reach below hold for all the sets of parameters investigated. In fact, in §5.5 we demonstrate that our results are independent of the set of parameters used, and are characteristic of nutrient-dependent AI production.

5.4 Results and Discussion

We performed pair-wise competitions between the QS strategy with oxygen-dependent AI production and fixed strategies with matrix bias ranging from 0 to 0.9 (in increments of 0.1). An example of snapshots at different time points in an example of simulations of pairwise competitions can be seen in Fig. 5.2.

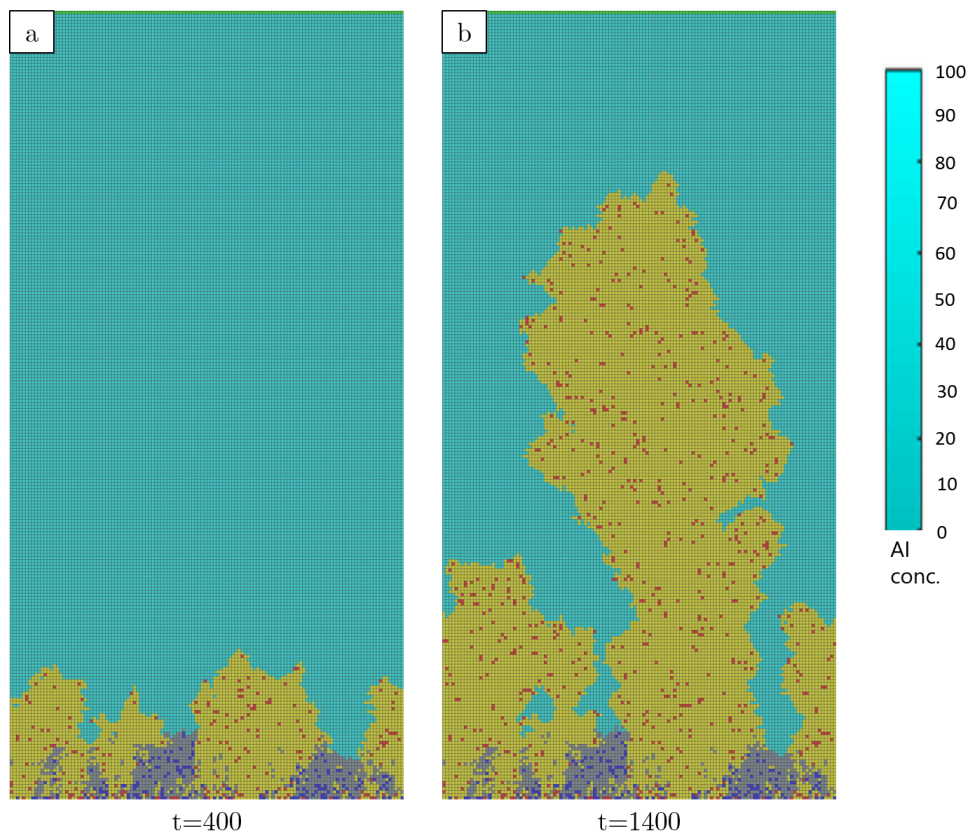


Figure 5.2: Snapshots of a simulation of pairwise competition between a nutrient-dependent AI-producing QS strategy and a fixed-strategy (differentiated by color). Blue cells produce and detect AI while red cells have a matrix bias of 0.6. The left snapshot is after 400 timesteps and the right snapshot is after 1400 timesteps. Yellow and grey squares are occupied by matrix and cyan squares are unoccupied. The shades of cyan squares indicate the AI concentration at the sites.

To evaluate the competitive advantage of the two strategies, we looked at the ratio, $n(\text{QS})/n(\text{Fixed})$, where $n(\text{QS})$ is the number of cells of the nutrient-dependent AI-producing QS strategy, and $n(\text{Fixed})$ is the number of cells of the fixed strategy. We repeated many simulations for each fixed strategy. The average results from all simulations can be seen in the plot in Fig. 5.3. For a comparison, the results from the competition of cells with the constitutive AI-producing strategy, described in §4, is also plotted. Each point in the plot indicates the log of the ratio, $n(\text{QS})/n(\text{Fixed})$, at the end of the simulation, averaged over all the simulations performed for that pair of values. Over 50 simulations were performed for competitions between cells performing QS and each fixed strategy.

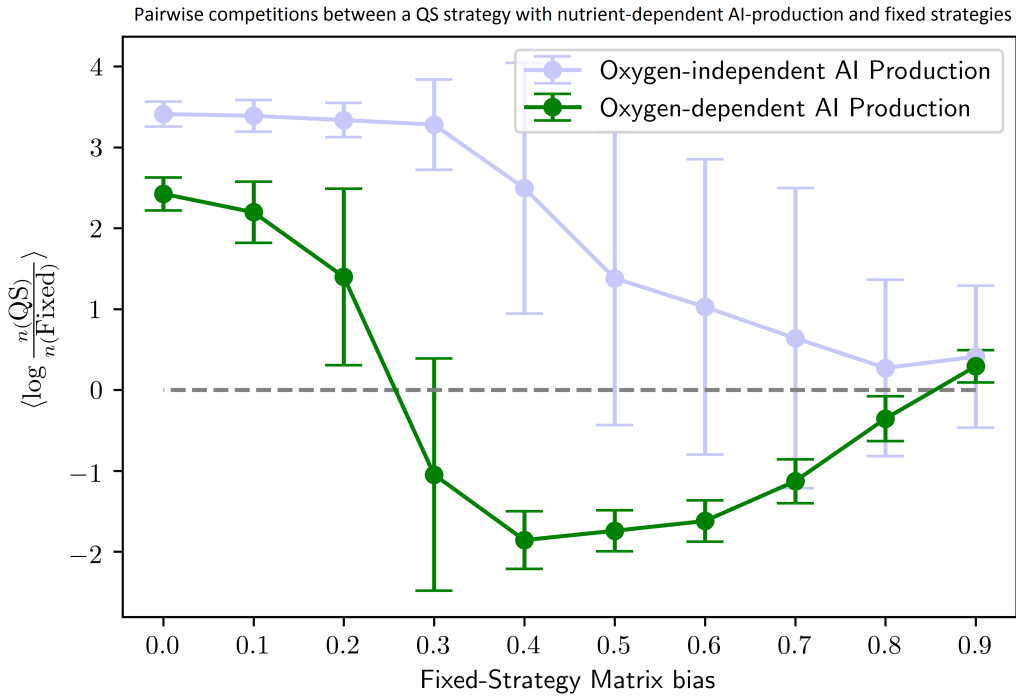


Figure 5.3: Logarithm of the final ratio of number of QS cells with nutrient-dependent AI-production to number of fixed strategy cells (indicated by column number), averaged over many simulations. The mean of the logarithm of the ratio of number of cells for constitutive AI-producing QS strategy in competition with fixed strategies is also plotted. All error bars are standard deviations. The grey dashed line corresponds to a y-value of zero.

Thus, we find that if AI production is dependent on the local O_2 concentrations, it does not gain a competitive advantage against fixed strategies. This result was obtained for a large range of parameters that exhibited switch-like transition between high matrix production and low matrix production. Though it was possible to find parameters such that the QS strategy performed better than fixed strategies, such a QS strategy did not exhibit a switch-like transitions between high matrix bias and low matrix bias.

We find that the reason why nutrient-dependent QS did not perform as well as QS with constitutive AI production is because nutrient-dependent QS cells were not

able to detect changes in cell density. As the number of cells with O_2 availability was limited to the edge of the biofilm, there were never enough AI producing cells. Initially, when there were few cells, AI production was high per cell, but over time though there were more cells, the number of cells with access to O_2 reduced and AI production per cell was low. As a result, we find that the AI concentrations did not change over time until the cells with fixed strategies outcompeted the QS cells and extinguished access to O_2 (see Fig 5.4).

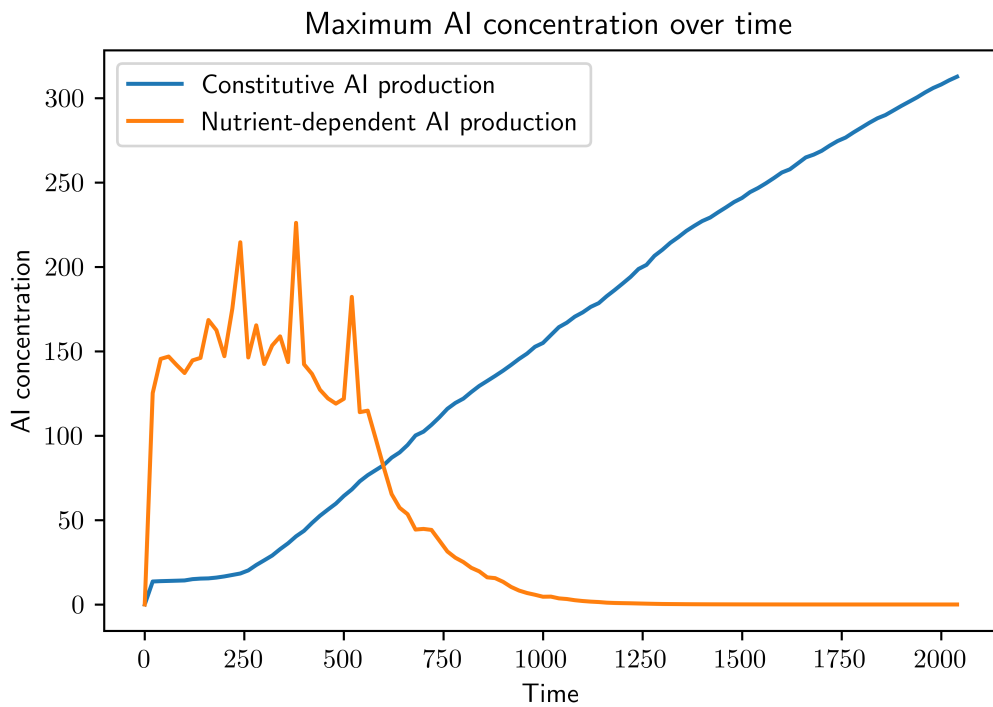


Figure 5.4: Maximum AI concentration in the entire simulation domain over time for constitutive AI production and nutrient-dependent AI production. Both strategies were placed in a pairwise competition with fixed strategies with a matrix bias of 0.4. This plot was obtained for one simulation in each case, but was typical of most simulations for each form of QS.

In Fig. 5.4, we see that if AI production is nutrient-dependent, the maximal AI

concentration is very high right from the start. These maximal values were found at the locations of the cells. Thus, the cells were essentially detecting the AI output by themselves. The sharp spikes in AI concentration values were due to the solitary presence of an AI producing cell at the edge of the biofilm (which it reached due to its high matrix bias at low AI concentrations). However, these spikes made the QS cells switch to a low matrix bias, and the fixed strategy cells reached the edge of the biofilm as they now had higher matrix biases than the QS cells. Thus, we find that after around 750 timesteps, the QS strategy with nutrient-dependent AI production was outcompeted by the fixed strategies. However, in the case of constitutive AI production, the maximal AI concentration increased with cell number and was roughly monotonic and all the cells collectively respond with a change in gene expression after around 250 timesteps.

Therefore, sensing the local AI concentration for nutrient-dependent AI production is not indicative of whether the bacteria of that strategy have a competitive advantage in accessing the nutrient. Thus, the cells cannot switch their matrix bias from a high value to a low value, and QS is not helpful. This result was found for a wide range of parameters that exhibited switch-like transitions from high matrix bias to low matrix bias. In fact, we find that this result is not unique even to the 2D models being studied. We find an analytic biophysical limit for the dynamic range of QS in three dimensions.

5.5 Analytic Derivation of the Biophysical Limit for the Dynamic Range of QS in 3D

We consider QS bacteria in a solution with a diffusive solute, such as O_2 . Though this result holds for any nutrient, for convenience we will refer to our nutrient as O_2 . If we assume that there is a constant bulk concentration of O_2 very far away with a value of c_∞ , and that the cell has a constant concentration of O_2 at the boundaries,

the system can be described as follows:

$$\frac{\partial c}{\partial t} = D_{O_2} \nabla^2 c \quad (5.1)$$

where c is the concentration of O_2 at a point and D_{O_2} is the diffusion constant of oxygen in the medium. Thus, at steady state for spherical coordinates (assuming spherical symmetry) we have that

$$\frac{D_{O_2}}{r^2} \frac{\partial}{\partial r} \left(r^2 \frac{\partial c}{\partial r} \right) = 0 \quad (5.2)$$

One of the solutions to Eq. 5.2 is that c is some constant, say c_1 . Another solution to Eq. 5.2 is that $r^2 \frac{dc}{dr}$ is some constant, say c_2 . In the latter case, we have that

$$\frac{dc}{dr} = \frac{c_2}{r^2} \quad (5.3)$$

where c_2 is some constant. By solving Eq. 5.3 and then adding the two solutions to Eq. 5.2, we have that

$$c(r) = \frac{-c_2}{r} + c_1 \quad (5.4)$$

where the two constant variables are combined to give c_1 .

By solving Eq. 5.4 for the boundary condition that $c(\infty) = c_\infty$, we have that $c_1 = c_\infty$.

$$\Rightarrow c(r) = \frac{-c_2}{r} + c_\infty \quad (5.5)$$

Here, we require that $r \geq r_0$ where r_0 is the radius of the cell (as the oxygen concentration within the cell cannot easily be solved by flux balance), and by rearranging, we can relate c_2 to the O_2 concentration at the boundary of the cell:

$$c_2 = (c_\infty - c(r_0))r_0 \quad (5.6)$$

Now, by Fick's First Law, we have that the amount of O_2 entering the cell per unit time, J_{O_2} , is given by

$$J_{O_2} = D_{O_2} \oint_C \nabla c \cdot ds \quad (5.7)$$

(where C is used to denote the boundary of the cell) But $\nabla c = \frac{c_2}{r^2}$ We note that here we are assuming that the concentration gradient of O_2 is continuous and uniform at the boundary of the bacteria. By assuming that the cell is spherical¹

$$\implies J_{O_2} = 4\pi D_{O_2} r_o^2 \frac{c_2}{r_o^2} = 4\pi D_{O_2} c_2 \quad (5.8)$$

If we suppose that the cell converts b molecules of O_2 to 1 molecule of AI, we have that the cell produces $\frac{4\pi D c_2}{b}$ molecules per unit time. Again, by Fick's First Law, we have that

$$\frac{4\pi D_{O_2} c_2}{b D_{AI}} = - \oint_C \nabla g(r) ds \quad (5.9)$$

where $g(r)$ is the concentration of [AI] at a radial distance r from the center of the cell; and D_{AI} is the Diffusion Constant for AI.

Assuming that the concentration of AI is constant across the boundary of the cell,

$$\frac{4\pi D_{O_2} c_2}{b D_{AI}} = -4\pi r_o^2 \nabla g(r_o) \quad (5.10)$$

$$\implies \nabla g(r_o) = -\frac{D_{O_2} c_2}{b D_{AI} r_o^2} \quad (5.11)$$

$$\implies g(r) = \frac{D_{O_2} c_2}{b D_{AI} r} + c_3 \quad (5.12)$$

If we assume that the concentration of AI very far from the source is 0, we have that

$$g(\infty) = 0 \implies c_3 = 0 \quad (5.13)$$

Thus, we have that in the presence of a single cell,

$$\implies g(r) = \frac{D_{O_2} c_2}{b D_{AI} r}, \quad r \geq r_o \quad (5.14)$$

Further, we have that

$$c(r) + \frac{b D_{AI}}{D_{O_2}} g(r) = c_\infty \quad r \geq r_o \quad (5.15)$$

Further, Eq. 5.15 is valid for any vector \vec{r} .

¹This result holds for cells of all shapes whose surface area has a r^2 dependence on the radius, up to a constant factor. The r^2 dependence is valid for shapes for whom the concept of a radius can be well defined, such as spheres, cylinders and cones.

As diffusion is a linear operator for each cell, the total distribution of the concentration values in the system is the superposition of the distribution of all the cells, centered at the locations of their respective cells. Thus, by using the same boundary conditions for all cells at infinity, we get that

$$c(\vec{r}) + \frac{bD_{\text{AI}}}{D_{\text{O}_2}} g(\vec{r}) = c_\infty \quad (5.16)$$

Above, we only require that $\|\vec{r} - \vec{r}_i\| \geq r_0$ where \vec{r}_i is the center of any cell.

Now, we have that

$$\max(g(\vec{r})) = \frac{D_{\text{O}_2}}{bD_{\text{AI}}} c_\infty$$

which is the case when $c(\vec{r}) = 0$. Further, we have that for just one cell, $c(r_0) = c_\infty - \frac{c_2}{r_0}$

$$\implies g(\vec{r}) = (c_\infty - c(r_0)) \frac{D_{\text{O}_2}}{bD_{\text{AI}}} \quad (5.17)$$

We can define the dynamic range DR , as the ratio of the maximum AI concentration possible to the concentration of AI in the boundary of one cell, when it is the only cell.

$$DR = \frac{D_{\text{O}_2} c_\infty}{bD_{\text{AI}}} \frac{bD_{\text{AI}}}{D_{\text{O}_2}(c_\infty - c(r_0))} = \frac{c_\infty}{c_\infty - c(r_0)} \quad (5.18)$$

Now, assuming that the intake of O_2 is proportional to the O_2 concentration at any point, the flux of O_2 , j , at the boundary of the cell is given by

$$J_{\text{O}_2} = -c(r_0)j \quad (5.19)$$

where j is the rate of intake of O_2 per unit volume (with units of vol./time).

Equating Eq. 5.8 and Eq. 5.19, we have that

$$4\pi D_{\text{O}_2} c_2 = c(r_0)j = \left(c_\infty - \frac{c_2}{r_0}\right) j \quad (5.20)$$

$$\implies 4\pi D_{\text{O}_2} = \left(\frac{c_\infty}{c_2} - \frac{1}{r_0}\right) j \quad (5.21)$$

$$\implies \frac{c_\infty}{c_2} = \frac{4\pi D_{\text{O}_2}}{j} + \frac{1}{r_0} \quad (5.22)$$

$$\implies DR \equiv \frac{[AI]_{\max}}{[AI]_{\text{one cell}}} = \frac{c_\infty}{r_2 c_2} = \frac{4\pi D_{O_2} r_0}{j} + 1 \quad (5.23)$$

Thus, to allow for a larger range of AI concentration values, we would want the dynamic range to be as large as possible. Thus, we want r_0 to be as large as possible, and j to be as small as possible.

We can now relate this to the penetration depth of O_2 in a homogeneous culture of bacteria, and ask the question, what are the limits on the penetration depth for a large range in signaling? The penetration depth λ is given by $\sqrt{\frac{D}{w}}$ where w is the coefficient of decay of O_2 in a system. It's to be noted that this expression for penetration depth only holds within the culture, and the boundary value for the decay problem is taken to be c_∞ . In this case, O_2 does not decay but is consumed by the cells. Thus, we have that w is the product of uptake per cell and the density of cells. $w = j\rho$ where ρ is the local cell density

$$\begin{aligned} &\implies \lambda^2 = \frac{D}{j\rho} \\ &\implies DR = \frac{4\pi j \rho \lambda^2 r_0}{j} + 1 = 1 + 4\pi \rho \lambda^2 r_0 \end{aligned} \quad (5.24)$$

To get a rough estimate, a typical *E. coli* cell has a radius of approximately $1\mu\text{m}$ [21]. QS has been shown to occur at densities of 5×10^8 cells/ml in *E. coli* [31]. The O_2 penetration depth for *P. aeruginosa* was found by microelectrode studies [32] to be $30\ \mu\text{m}$. For these values, we get that $DR = 5.65$. We stress that Eq. 5.24 is the theoretical upper bound for the dynamic range in such a system, and in real biological systems, the actual value may be lower than this upper bound.

We note that Eq. 5.24 holds for any QS bacteria, and for any nutrient-limited dense culture of cells. Further, no assumptions were made regarding the nutrient, other than that it diffuses into the cluster from very far away.

Chapter 6

Conclusion

6.1 Summary of Results

In this investigation, we explored the competitive advantage afforded by matrix production in accessing a diffusive nutrient in bacterial biofilms. We showed that the optimal matrix bias for our configuration would be around 0.7. We were then able to show that, if AI production is constitutive, bacteria can outcompete any fixed strategy by using QS to regulate matrix production. Further, bacteria can significantly increase their growth rate by using QS to divert its resources away from matrix production and towards reproduction.

However, we find that if AI production is dependent on nutrient availability, then QS does not afford any benefit. We understand this analytically as a biophysical limit to the dynamic range of QS with nutrient-limited AI production. The limit was described in terms of both physical parameters and biological parameters.

6.2 Reconciling Quorum Sensing and the Biophysics Limit

QS is observed in many bacterial biofilms and other nutrient-limited environments with bacteria. Thus, the bacteria either must perform QS with the limited dynamic range of AI concentrations, or operate outside of the assumptions underlying the

biophysical limit. Performing QS efficiently in the limited dynamic range can be difficult as the sensing would be sensitive to small changes in AI concentrations. Thus, for stable sensing, bacteria must perform QS with a wide dynamic range.

A possibility for some species of bacteria in certain environments is that due to the biological conditions in which they operate, the dynamic range is high. For example, *Vibrio fischeri* occur at densities as high as 10^{10} to 10^{11} cells per ml [33]. As the dynamic range has a term linear to the density of the cells, high densities will allow for large dynamic ranges. For other bacteria, the dynamic range afforded by their biological parameters may suffice for QS to perform the functions it does.

The other strong possibility is that QS is a privileged process and occurs even at low nutrient environments. As QS is so crucial to the survival of many bacteria, QS may be a high priority process such that the conversion of oxygen to AI is effectively non-linear. In §5.1, we discussed how the signaling molecule in some QS systems, such as acyl-homoserine lactone (acyl-HSL), is made by a process that reflects an active physiological state. Parsek et al. discuss one of the substrate for acyl-HSL synthesis, S-adenosyl methionine (SAM). SAM is a product of the one-carbon metabolism cycle, and thus Parsek et al. hypothesize that the availability of SAM will depend on the metabolic state of the cell. However, recently, Ye et al. showed that serine catabolism through the one-carbon metabolism cycle is induced during hypoxia [34] [35]. Thus, it is possible for SAM to be present even in low oxygen levels and for acyl-HSL to be produced. This example indicates that there may be many other QS systems where the pathways that lead to the production of the signaling molecule are not metabolically slaved.

Further, we assume in this case that the only information available to the bacteria to perform QS is the local AI concentration. Another way of getting around the limited dynamic range would be to exploit the availability of other information, such as gradients or memory. We also assume that QS is the only form of communication within bacteria. Several other forms of communication have been observed in bacteria,

such as ion channel mediated electrical signaling that is extremely important for spatial dynamics and nutrient sharing in bacterial biofilms [36].

Some investigators also argue that QS signals does not entail just communication, but also other interactions such as cues and chemical manipulations. This perspective is based on ecological and evolutionary perspective, and is specific to a small class of bacteria [37]. In general, we believe that it is a combination of many ecological, physical, biological and chemical factors that allow for QS to function in nutrient limited environments.

6.3 Assumptions behind the Agent-Based Model

Our analytic result was motivated by results from a series of agent-based models of biofilm growth and communication. These results were based on many simplifying assumptions, which may or may not misrepresent the true dynamics of growth and communication in a biofilm. In each case, we believe that our assumption does not affect the large-scale emergent phenomena in biofilms.

The most evident of these assumptions is that bacterial cells occupy exactly one lattice site. This cannot be true as bacteria change volume over time as they grow, and two bacteria can be of vastly different volumes. Further, we assume that bacteria produce exactly enough extra-cellular matrix in one time-step to fill one lattice site, which is also untrue. These assumptions were necessary to operate in the lattice geometry, which allowed for significant reductions in the runtime. However, as the biofilms are much larger than individual cells, we believe that these assumptions do not affect the large scale spatial structure of the biofilm, and videos from simulations support this belief.

We also used simple kinematics with O_2 consumption rates and AI production rates. This is not true in real biological systems. The O_2 consumption rates are more akin to Michaelis-Menten kinematics. However, this assumption was necessary to keep

the reaction diffusion equation linear. We believe that as nutrients are limited in a biofilm, oxygen consumption rates are in the linear regime.

We also assume that the timescale of reproduction and matrix production is significantly longer than that of equilibration for the reaction diffusion equation. This is a fairly safe assumption, as the time scales for equilibration are estimated to be 3-5 minutes [18], while a single time step for reproduction represents closer to 1 hour in systems such as *E. coli*. However, the time scales for equilibration grow as the surface area of the biofilm [18], and thus for large sparse biofilms, this assumption may not hold.

6.4 Limitations and Future Steps

An important limitation of our ABM simulations has been that they have been performed in two dimensions. However, bacterial biofilms are three dimensional structures in three dimensional environments. And spatial structure in the third dimension can be crucial in demonstrating emergent phenomenon. For example, due to surface adhesion, bacteria clump together perpendicular to the interface whereas their movement along the interface is slow. An understanding of important spatial features of biofilms that emerge in three dimensions has been developing ([38]) and are thus lost in our simulations. This limitation was purely the result of a lack of computational tools available to use ABMs in three dimensions, and future efforts must be made to address this. However, it must be noted that the analytic result detailed in §5.5 holds for three dimensions, and is independent of the results from ABMs in Chapters 2-5.

Another important limitation was that the only metric used in the analysis was ratio of the cell count at the end of the simulation. However, this may not be indicative of the fitness of the strategy at the end of the simulation. For example, the cells at the center of the biofilm may be dead and no longer relevant. An understanding of the metrics that determine the evolutionary fitness of the strategy will aid this

investigation in better understanding the competitive advantage of the strategies.

6.5 Experimental Verification

Due to the many applications of targeting the QS mechanism, it is crucial to understand how bacteria get around the biophysical limit in Eq. 5.24. An experimental verification of the hypothesis that AI production is not metabolically slaved is critical to understanding QS pathways. These pathways could be targeted for many antibiotic and probiotic interventions. One experiment to test this would be to check for AI production in different nutrient-limited environments. Nutrients that could be limited include oxygen and glucose. Though limiting oxygen would require an anaerobic chamber and is a difficult experiment, limiting glucose availability should be possible with relatively simple experiments using a chemostat.

Chapter 7

References

- [1] Jost Wingender, Thomas R Neu, and Hans-Curt Flemming. What are bacterial extracellular polymeric substances? In *Microbial extracellular polymeric substances*, pages 1–19. Springer, 1999.
- [2] J William Costerton, Philip S Stewart, and EP Greenberg. Bacterial biofilms: a common cause of persistent infections. *Science*, 284(5418):1318–1322, 1999.
- [3] Luanne Hall-Stoodley, J William Costerton, and Paul Stoodley. Bacterial biofilms: from the natural environment to infectious diseases. *Nature Reviews Microbiology*, 2(2):95–108, 2004.
- [4] Don Monroe. Looking for chinks in the armor of bacterial biofilms. *PLoS Biol*, 5(11):e307, 2007.
- [5] Bonnie L Bassler and Richard Losick. Bacterially speaking. *Cell*, 125(2):237–246, 2006.
- [6] Hans-Curt Flemming and Jost Wingender. The biofilm matrix. *Nature Reviews Microbiology*, 8(9):623–633, 2010.
- [7] Carey D Nadell, Joao B Xavier, and Kevin R Foster. The sociobiology of biofilms. *FEMS microbiology reviews*, 33(1):206–224, 2009.

- [8] Dirk De Beer, Paul Stoodley, Frank Roe, and Zbigniew Lewandowski. Effects of biofilm structures on oxygen distribution and mass transport. *Biotechnology and bioengineering*, 43(11):1131–1138, 1994.
- [9] Ann M Stevens and E Peter Greenberg. Quorum sensing in vibrio fischeri: essential elements for activation of the luminescence genes. *Journal of Bacteriology*, 179(2):557–562, 1997.
- [10] L Lin and E Meighen. Bacterial bioluminescence biochemistry and molecular biology, 2009.
- [11] Joao B Xavier and Kevin R Foster. Cooperation and conflict in microbial biofilms. *Proceedings of the National Academy of Sciences*, 104(3):876–881, 2007.
- [12] Carey D Nadell, Joao B Xavier, Simon A Levin, and Kevin R Foster. The evolution of quorum sensing in bacterial biofilms. *PLoS Biol*, 6(1):e14, 2008.
- [13] David Bruce Borenstein. *A multi-agent approach to the evolution of microbial populations in the presence of spatially structured social interaction*. PhD thesis, Princeton University, 2015.
- [14] Dirk Helbing, Illés Farkas, and Tamas Vicsek. Simulating dynamical features of escape panic. *Nature*, 407(6803):487–490, 2000.
- [15] Carey D Nadell, Kevin R Foster, and João B Xavier. Emergence of spatial structure in cell groups and the evolution of cooperation. *PLoS Comput Biol*, 6(3):e1000716, 2010.
- [16] Knut Drescher, Carey D Nadell, Howard A Stone, Ned S Wingreen, and Bonnie L Bassler. Solutions to the public goods dilemma in bacterial biofilms. *Current Biology*, 24(1):50–55, 2014.

- [17] Ronnie Nøhr Glud, Cecilia Maria Santegoeds, Dirk De Beer, Oliver Kohls, and Niels Birger Ramsing. Oxygen dynamics at the base of a biofilm studied with planar optodes. *Aquatic Microbial Ecology*, 14(3):223–233, 1998.
- [18] Philip S Stewart. Diffusion in biofilms. *Journal of bacteriology*, 185(5):1485–1491, 2003.
- [19] David B Borenstein. Diffusion and cooperation, 2013.
- [20] Jonathan M Monk, Anna Koza, Miguel A Campodonico, Daniel Machado, Jose Miguel Seoane, Bernhard O Palsson, Markus J Herrgård, and Adam M Feist. Multi-omics quantification of species variation of escherichia coli links molecular features with strain phenotypes. *Cell Systems*, 3(3):238–251, 2016.
- [21] HE Kubitschek and JA Friske. Determination of bacterial cell volume with the coulter counter. *Journal of bacteriology*, 168(3):1466–1467, 1986.
- [22] Ralph T Ferrell and David M Himmelblau. Diffusion coefficients of nitrogen and oxygen in water. *Journal of chemical and engineering data*, 12(1):111–115, 1967.
- [23] U.S. Geological Survey. *National field manual for the collection of water-quality data: U.S. Geological Survey Techniques of Water-Resources Investigations*. U.S. Geological Survey, variously dated.
- [24] Klaus B Andersen and Kaspar von Meyenburg. Are growth rates of escherichia coli in batch cultures limited by respiration? *Journal of Bacteriology*, 144(1):114–123, 1980.
- [25] J áB Kaplan. Biofilm dispersal: mechanisms, clinical implications, and potential therapeutic uses. *Journal of dental research*, 89(3):205–218, 2010.
- [26] Matthew R Parsek and E Peter Greenberg. Sociomicrobiology: the connections between quorum sensing and biofilms. *Trends in microbiology*, 13(1):27–33, 2005.

- [27] Matthew R Parsek, Dale L Val, Brian L Hanzelka, John E Cronan, and E Peter Greenberg. Acyl homoserine-lactone quorum-sensing signal generation. *Proceedings of the National Academy of Sciences*, 96(8):4360–4365, 1999.
- [28] Margret I Moré, L David Finger, Joel L Stryker, et al. Enzymatic synthesis of a quorum-sensing autoinducer through use of defined substrates. *Science*, 272(5268):1655, 1996.
- [29] Wei Ding, Lorissa J Smulan, Nicole S Hou, Stefan Taubert, Jennifer L Watts, and Amy K Walker. s-adenosylmethionine levels govern innate immunity through distinct methylation-dependent pathways. *Cell metabolism*, 22(4):633–645, 2015.
- [30] John W Campbell and John E Cronan Jr. Bacterial fatty acid biosynthesis: targets for antibacterial drug discovery. *Annual Reviews in Microbiology*, 55(1):305–332, 2001.
- [31] Michael G Surette and Bonnie L Bassler. Quorum sensing in escherichia coli and salmonella typhimurium. *Proceedings of the National Academy of Sciences*, 95(12):7046–7050, 1998.
- [32] Karen D Xu, Philip S Stewart, Fuhu Xia, Ching-Tsan Huang, and Gordon A McFeters. Spatial physiological heterogeneity in pseudomonas aeruginosa biofilm is determined by oxygen availability. *Applied and environmental microbiology*, 64(10):4035–4039, 1998.
- [33] E Peter Greenberg. Cell density-dependent gene expression controls luminescence in marine bacteria and virulence in several pathogens. *ASM News*, 63(7).
- [34] Jiangbin Ye, Jing Fan, Sriram Venneti, Ying-Wooi Wan, Bruce R Pawel, Ji Zhang, Lydia WS Finley, Chao Lu, Tullia Lindsten, Justin R Cross, et al. Serine catabolism regulates mitochondrial redox control during hypoxia. *Cancer discovery*, 4(12):1406–1417, 2014.

- [35] Inmaculada Martínez-Reyes and Navdeep S Chandel. Mitochondrial one-carbon metabolism maintains redox balance during hypoxia. *Cancer discovery*, 4(12):1371–1373, 2014.
- [36] Arthur Prindle, Jintao Liu, Munehiro Asally, San Ly, Jordi Garcia-Ojalvo, and Gürol M Süel. Ion channels enable electrical communication in bacterial communities. *Nature*, 527(7576):59–63, 2015.
- [37] Laurent Keller and Michael G Surette. Communication in bacteria: an ecological and evolutionary perspective. *Nature Reviews Microbiology*, 4(4):249–258, 2006.
- [38] Jing Yan, Andrew G Sharo, Howard A Stone, Ned S Wingreen, and Bonnie L Bassler. Vibrio cholerae biofilm growth program and architecture revealed by single-cell live imaging. *Proceedings of the National Academy of Sciences*, page 201611494, 2016.
- [39] Julie Theriot Hernan G. Garcia Rob Phillips, Jane Kondev and Nigel Orme. *Physical Biology of the Cell*. Garland Science, 2009.
- [40] Satish Balay, Shrirang Abhyankar, Mark F. Adams, Jed Brown, Peter Brune, Kris Buschelman, Lisandro Dalcin, Victor Eijkhout, William D. Gropp, Dinesh Kaushik, Matthew G. Knepley, Lois Curfman McInnes, Karl Rupp, Barry F. Smith, Stefano Zampini, Hong Zhang, and Hong Zhang. PETSc Web page. <http://www.mcs.anl.gov/petsc>, 2016.
- [41] Satish Balay, Shrirang Abhyankar, Mark F. Adams, Jed Brown, Peter Brune, Kris Buschelman, Lisandro Dalcin, Victor Eijkhout, William D. Gropp, Dinesh Kaushik, Matthew G. Knepley, Lois Curfman McInnes, Karl Rupp, Barry F. Smith, Stefano Zampini, Hong Zhang, and Hong Zhang. PETSc users manual. Technical Report ANL-95/11 - Revision 3.7, Argonne National Laboratory, 2016.
- [42] Satish Balay, William D. Gropp, Lois Curfman McInnes, and Barry F. Smith. Efficient management of parallelism in object oriented numerical software libraries.

- In E. Arge, A. M. Bruaset, and H. P. Langtangen, editors, *Modern Software Tools in Scientific Computing*, pages 163–202. Birkhäuser Press, 1997.
- [43] Joseph L Doob. Topics in the theory of markoff chains. *Transactions of the American Mathematical Society*, 52(1):37–64, 1942.
- [44] David Borenstein. *Nanoverse documentation*. nanoverse, v1.0.0-a10 edition, apr 2016.
- [45] Jeremy S Webb, Lyndal S Thompson, Sally James, Tim Charlton, Tim Tolker-Nielsen, Birgit Koch, Michael Givskov, and Staffan Kjelleberg. Cell death in *pseudomonas aeruginosa* biofilm development. *Journal of bacteriology*, 185(15):4585–4592, 2003.
- [46] Angela H Finney, Robert J Blick, Katsuhiko Murakami, Akira Ishihama, and Ann M Stevens. Role of the c-terminal domain of the alpha subunit of rna polymerase in luxr-dependent transcriptional activation of the lux operon during quorum sensing. *Journal of bacteriology*, 184(16):4520–4528, 2002.
- [47] William G Characklis and Kevin C Marshall. *Biofilms*. John Wiley\& Sons, 1990.
- [48] Philip S Stewart and Michael J Franklin. Physiological heterogeneity in biofilms. *Nature Reviews Microbiology*, 6(3):199–210, 2008.

Appendices

Appendix A

Supplementary Information

A.1 The Algorithm behind Nanoverse

The algorithm behind performing any simulation on Nanoverse can be enumerated as follows [19]

1. Begin the simulation with some defined initial condition, including initial location of agents.
2. Calculate the steady-state concentration of the solutes in the environment
3. Determine the reactions of the agents according to local environment
4. Update the location of agents on the lattice
5. Repeat steps 2-4 until a specified halt condition is reached

A.2 Solving the Reaction-Diffusion Equation

Note: This section is based on the notes of David Borenstein, the creator of Nanoverse, which can be found in their original at [19] and [13].

The operations that can be performed on the solute layer are a flux (either positive and negative) and a first order scaling. The net flux at a point is designated by α , and the net scaling is denoted by β . The solute also diffuses with a diffusion constant

of D . Thus, the concentration of the solute satisfies [13]:

$$\frac{\partial c(x, y)}{\partial t} = D \nabla^2 c(x, y) + \alpha(x, y) - \beta(x, y)c(x, y)$$

In general, the diffusion operator matrix can be obtained using center-space finite differencing [19]:

$$\frac{\partial c}{\partial t} = D \left(\frac{\partial^2 c}{\partial x^2} + \frac{\partial^2 c}{\partial y^2} \right) \approx \frac{c(t + \Delta t) - c(t)}{\Delta t}$$

and

$$\frac{\partial^2 c}{\partial x^2} \approx \frac{c(x + \Delta x, y, t) - 2c(x, y, t) + c(x - \Delta x, y, t)}{(\Delta x)^2}$$

We let $\Delta x = \Delta y$. Thus,

$$c(x, y, t + \Delta t) = c(x, y, t) - 4 \frac{D \Delta t}{(\Delta x)^2} c(x, y, t) + \frac{D \Delta t}{(\Delta x)^2} \sum_{(x', y') = (x \pm 1, y \pm 1)} c(x', y', t)$$

It must be noted that this step is, by far, the most computationally expensive step of the simulation, and we take a few additional steps to reduce the time complexity of this step.

A.2.1 Superposition Method

Solute production, diffusion and decay is a linear operator that is identical for each cell. Hence the total distribution of the solute is the superposition of the distributions of all the cells, adjusted for their location in the grid. This fact was used to increase the computational efficiency of the simulation [19].

The total distributions could naively be precomputed by solving an $N \times N$ matrix, where N is the number of cells in the system. However, most iterative matrix solvers require matrix multiplication. The best multiplication methods have a best-case time complexity of $O(n^{2.3})$, and are often of even higher orders. The procedure described above requires that this be done in each time step, and this would make the computations incredibly slow. However, precomputation requires that only one matrix be solved [19].

By precomputing this distribution and storing it in a lookup table, adding the contribution of a single cell at each site requires constant time. Therefore, adding the contribution of a single cell to the entire system is an $O(N)$ step, and calculating the steady-state distribution for an arbitrary configuration of M cells has complexity $O(N \cdot M)$ (by necessity, $M \leq N$) [19].

A.2.2 Linear Solvers

The linear solvers solve the reaction-diffusion equation at each step. The solver used for this set of results was PETSc [40]. PETSc was chosen due to its large suite of parallel linear solvers and ODE integrators that are easily used in application codes written in C.

Appendix B

Supplementary Figures

Though in our investigation we ignored matrix production, it may be instructive to look at the production of matrix by each strategy.

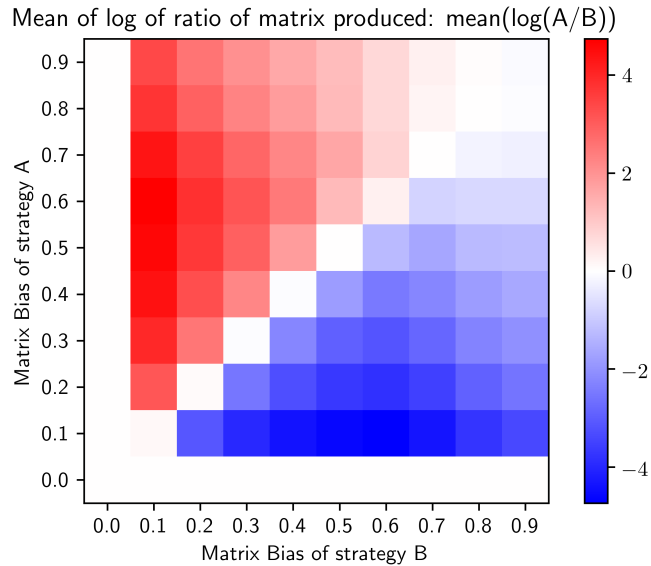


Figure B.1: Logarithm of the final ratio of volume of matrix produced by strategy A cells (indicated by row number) to the volume of matrix produced by strategy B cells (indicated by column number), averaged over many simulations.

We note that it is not necessarily the strategies with high matrix bias that produce the most matrix, as they can very quickly lose access to nutrient. However, as most of the volume is occupied by matrix, Fig. B.1 is very indicative of the proportion of the simulation domain occupied by different matrix biases and the matrix produced

by them.

The number of simulations performed to obtain the results in Fig. B.1 is the same as for the results in Fig. 3.2, and can be seen in 3.3. The standard deviation for each distribution can be seen in Fig. B.2

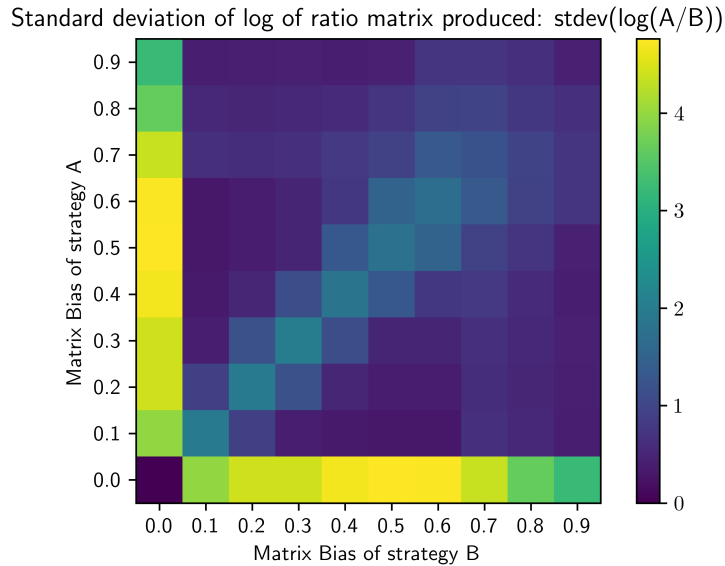


Figure B.2: Standard deviation of the distribution of logarithms of the final ratio of volume of matrix produced by strategy A cells (indicated by row number) to the volume of matrix produced by strategy B cells (indicated by column number).

We can also calculate the amount of biomass produced by each strategy by adding the matrix produced and the number of cells for each pair of strategies. The contributions of matrix and cells would be weighted by the relative cost of matrix production to reproduction. The amount of biomass produced is indicative of the resource usage by each strategy.

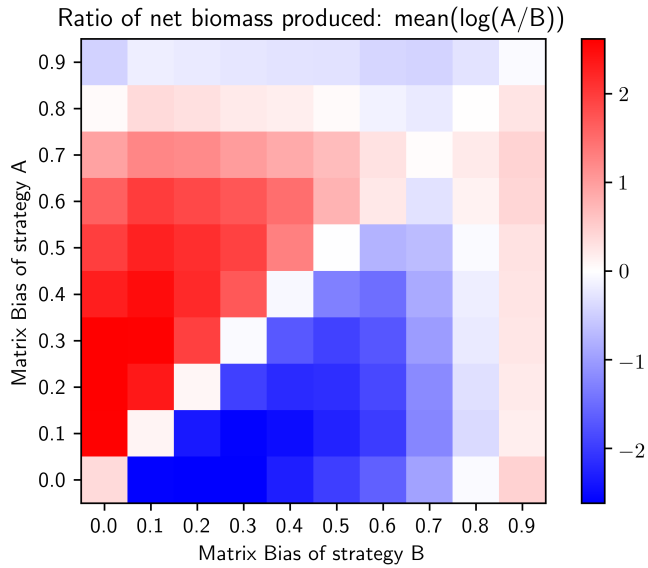


Figure B.3: Logarithm of the final ratio of biomass of strategy A cells (indicated by row number) to the biomass of strategy B cells (indicated by column number), averaged over many simulations.

Thus, we note that the ratio of actual resource consumption is almost identical to the ratio of cells present at the end of the simulation (see Fig. 3.2).

As discussed in Fig. 3.5, the number of timesteps taken to complete each simulation can vary greatly. In particular, for bacteria with large matrix biases, the simulation domain can very quickly be occupied as matrix production is cheaper per unit volume and, thus, much quicker than reproduction.

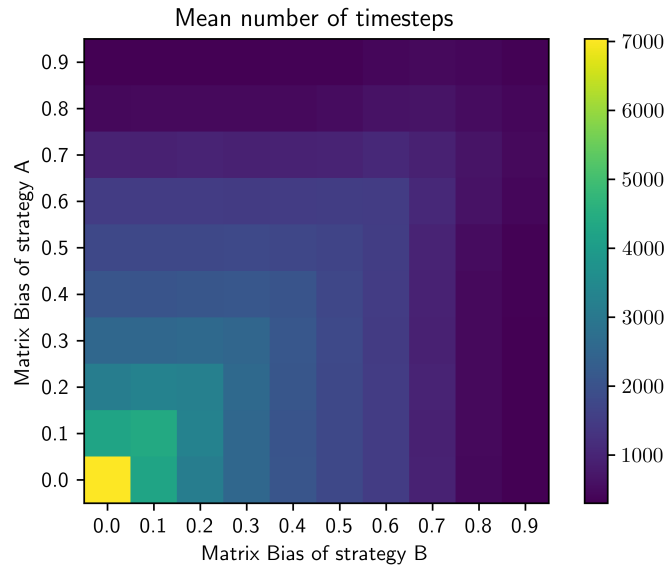


Figure B.4: The mean number of timesteps required to reach the halt condition for pairwise competitions between fixed strategies

The standard deviation of the distributions that were used to plot Fig. B.4 is given in Fig. B.5.

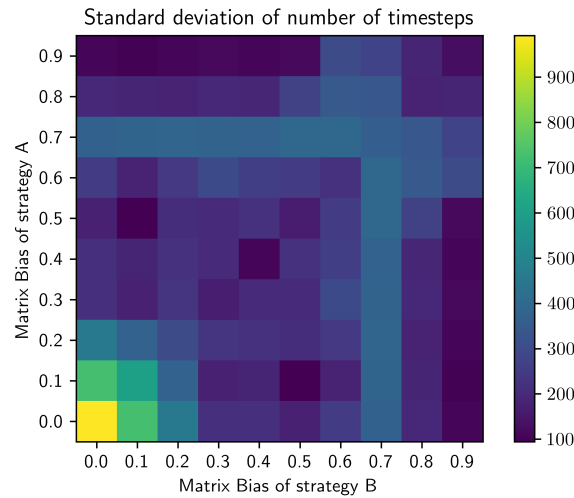


Figure B.5: The standard deviation of the number of timesteps required to reach the halt condition for pairwise competitions between fixed strategies

B.1 Parameter Dependence for Fixed Strategies

As mentioned in §2.3, we repeated our simulations with different numbers of cells at the beginning of the simulation. These are the results of simulations with 32 cells of each strategy placed randomly at the bottom row of cells. However, for sufficiently low initial number of cells, we expect different results as the strategies will not compete and grow independently.

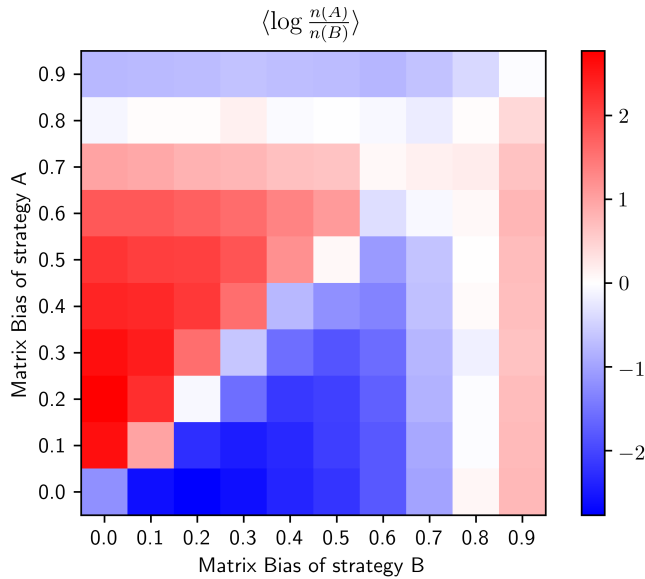


Figure B.6: Logarithm of the final ratio of number of strategy A cells (indicated by row number) to number of strategy B cells (indicated by column number), averaged over many simulations. Only 32 cells of each strategy were placed randomly at the bottom row of cells. Compare to Fig. 3.2 where 64 cells were placed.

These are the results of simulations where the cost of matrix production was only $1/3$ of the cost of matrix production.

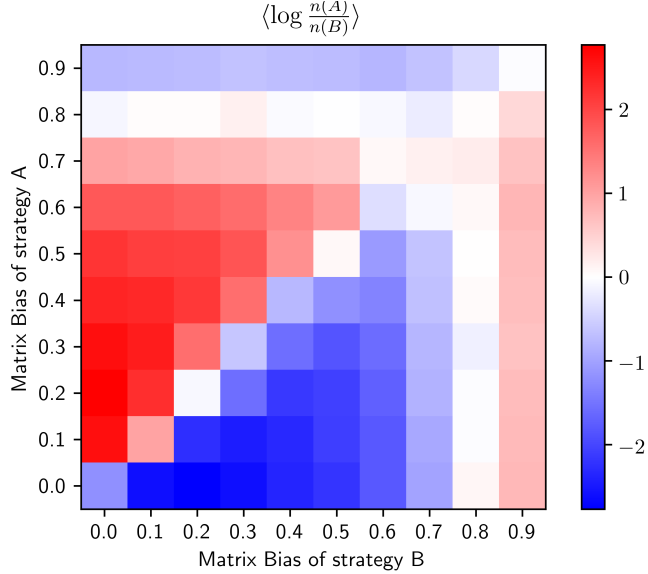


Figure B.7: Logarithm of the final ratio of number of strategy A cells (indicated by row number) to number of strategy B cells (indicated by column number), averaged over many simulations. The relative cost of reproduction to matrix production was 3. Compare to Fig. 3.2 where the cost was 7.

Thus, we see that strategies with high matrix biases were not as competitive as they were in the case of high relative cost. However, no clear pattern has emerged in this set of simulations.

These are the results of simulations where the diffusion constant was 0.01 as opposed to a diffusion constant was 0.005 used to obtain Fig. 3.2.

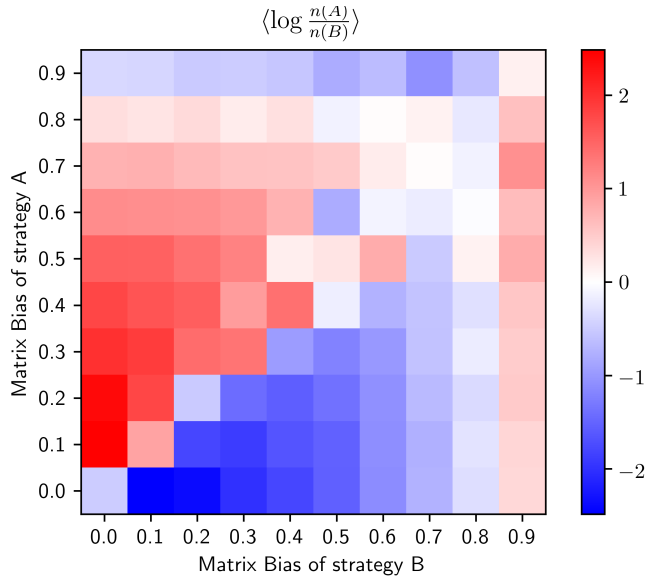


Figure B.8: Logarithm of the final ratio of number of strategy A cells (indicated by row number) to number of strategy B cells (indicated by column number), averaged over many simulations. The diffusion constant for the nutrient was 0.01. Compare to Fig. 3.2 where the diffusion constant was 0.005.

Similarly, we see that strategies with high matrix biases were not as competitive as they were in the case of low diffusion. However, no clear pattern has emerged in this set of simulations as no strategy is able to outcompete all other strategies for our set of parameters.

We also attempted to vary the consumption rate of consumption of oxygen to 0.005 from 0.01, which was the value used to obtain Fig. 3.2. However, no significant difference from Fig. 3.2 was observed. We believe that this is because the benefits of higher oxygen availability were shared among all members of the biofilm, and thus the log of the ratio is preserved.

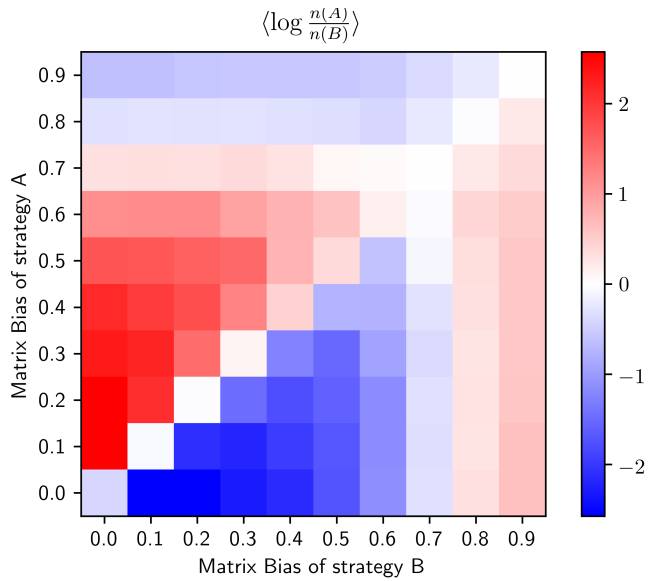


Figure B.9: Logarithm of the final ratio of number of strategy A cells (indicated by row number) to number of strategy B cells (indicated by column number), averaged over many simulations. The rate of consumption of nutrient was 0.005. Compare to Fig. 3.2 where the rate of nutrient consumption was 0.01.

Appendix C

Afterword on Relating Computer Models to Real Biological Systems

In this project, we use computer simulations to model bacterial biofilms and study their growth and spatial structure. One may ask if computer simulations are appropriate tools for studying bacteria. Considering the complexity of real biological systems, one would need tens of thousands of parameters to correctly describe the system and predict behaviors. Further, computer simulations must discretize space and time into large chunks - this is simply not the case in real biological systems. Bacteria simply do not live in idealized scenarios like those that most computational tools are typically used for. So why even try?

The answer is that by computationally evaluating a conceptual model, we hope to relate observable features of biological organisms, such as spatial structure and evolutionary success, to a small subset of physical parameters that we can control. These relations may not be entirely accurate in real biological systems, but hopefully they will provide us with an indication of the underlying mechanisms. Since we cannot search in parameter space for relations to tens of thousands of parameters, we try to isolate the crucial parameters that we believe drive the biological phenomena being studied (in this case, matrix production in biofilms). And then we hope that we can predict the qualitative and quantitative observables obtained through experiment (such as cell densities, gene expression, and concentrations).

Further, we believe that a search in parameter space for values which optimise

fitness will be reflected in observational values. Our reasoning behind this idea is that through millions and millions of years of evolution (which translates to hundreds of billions of generations in bacteria), competition in nature has driven biological organisms to the biophysical optima. If we do find that, for a given set of physical parameters, bacteria exist near some extremum, then we will have strong indication that we have isolated the physical parameters that drive evolution. If not, it would mean that there are some physical parameters and processes that we have ignored. In previous work, Nadell et al. (2010) have in fact demonstrated using multi-agent computational models that a small number of physical and biological parameters, including cell growth rate, nutrient availability, and nutrient diffusivity qualitatively alter the emergent structures of cell groups [15].

For this report as well, the main physical parameters are the rate of intake of nutrient, diffusion of nutrient and AI, the rate of growth (which determines the time scale of the simulation) and the radius of the cell (which determines the length scale of the simulation). By investigating different strategies, we will hopefully identify which strategies would lead to success. As physical and biological parameters often cannot be altered in *in vivo* experimental set-ups (for example, the diffusion coefficient of O₂ in water cannot be changed), simulations allow us to isolate dependence on different physical parameters.